SAND81-7015
Unlimited Release
UC-62

Stress Analysis for Spherically Curved Glass Reflectors

Shelltech Associates
Stanford, CA 94305

Prepared by Sandia National Laboratories, Albuquerque, New Mexico 87185
and Livermore, California 94550 for the United States Department
of Energy under Contract DE-AC04-76DP00789

Printed June 1981

Prepared for Sandia National Laboratories under Contract No. 62-6661

Sandia National Laboratories

Issued by Sandia National Laboratories, operated for the United States Department of Energy by Sandia Corporation.

Printed in the United States of America

Available from
National Technical Information Service
U. S. Department of Commerce
5285 Port Royal Road
Springfield, VA 22161

NTIS price codes
Printed copy: $8.00
Microfiche copy: A01

Distribution Category UC-62

SAND81-7015
Unlimited Distribution
Printed June 1981

STRESS ANALYSIS FOR SPHERICALLY CURVED GLASS REFLECTORS

Charles R. Steele
Nicholas Stephanou
Marielouise Steele
Drew Nelson

SHELLTECH ASSOCIATES
809 Tolman Drive
Stanford, California 94305

ABSTRACT

This report contains an analysis of the stresses that occur in elastically deformed, spherically curved glass mirrors for solar energy applications. Forming stresses, residual stresses, spring back deformation, and thermal stresses are analyzed. In addition, fracture mechanics and stress corrosion are discussed. Results are presented in generalized form for use in new designs.

Prepared for Sandia National Laboratories under Contract No. 62-6661

PREFACE

This is the Final Report of work conducted by SHELLTECH ASSOCIATES according to the Sandia Laboratories' Request for Quotation, Document Number 62-6661, dated June 12, 1980, responded to by the SHELLTECH Proposal, dated July 31, 1980. The Contract was awarded, dated October 1, 1980, and the work was performed during the period October 1, 1980 to December 31, 1980.

CONTENTS

NOTATION

Initially flat glass plate

w	=	Normal displacement
Φ	=	Airy stress function
E	=	Young's modulus
ν	=	Poisson's ratio
α	=	Coefficient of thermal expansion
h	=	Thickness
c	=	$h[12(1-\nu^2)]^{-\frac{1}{2}}$
L, L_y	=	Half-width and half-length of rectangular plate, in the x,y directions, respectively
b	=	Radius of circular plate
a	=	Radius of "hot spot"
p	=	Pressure
T	=	Temperature
R	=	Radius of curvature of spherical surface
σ_B	=	Bending stress
σ_D	=	Direct (membrane) stress
σ_{BO}	=	Nominal bending stress, $Eh/2(1-\nu)R$
σ_{DO}	=	Nominal direct stress, $Eb^2/8R^2$
w_0	=	Nominal displacement, $(x^2+y^2)/2R$

Sandwich panel

H	=	Thickness of honeycomb
G	=	Effective transverse shear modulus
h_s	=	Thickness of back plate
E_s	=	Young's modulus of back plate
D	=	Effective bending stiffness, $\cong H^2/(1-\nu^2)((Eh)^{-1}+(E_s h_s)^{-1})$
w_1	=	Springback displacement
β_1	=	Springback rotation of normal

1.0 INTRODUCTION

Glass surface panels with a spherical curvature are used to form hemispherical reflectors for fixed-mirror, distributed focus, solar energy collectors. It is especially important for these collectors to have high performance and low cost. A 65 foot diameter collector is shown in Fig. 1.1, and a proposed facility consisting of ten 200 foot diameter collectors is shown in Fig. 1.2. As reported by Perry (1980), E-Systems has undertaken an extensive program of development of the panels for the system in Fig. 1.1. The final production panel is shown in Fig. 1.3. A thin, flat mirror made from commercial-grade, float glass is elastically formed to the spherical contour and bonded to an impregnated paper honeycomb mounted on a steel backing plate.

The objective of the present study is to analyze the significant stresses and displacements in such a panel during fabrication and service. The results are in parametric form and should be useful for any future designs involving the cold forming of glass to a spherical surface. Our purpose is not to diagnose and correct any problems experienced in the Crosbyton Solar Power Project. However, the work at E-Systems related by Perry (1980) is drawn upon heavily, since this is our only source of practical experience and testing of this type of panel.

2.0 STRESS DURING FORMING

In this section we consider the process of deforming an initially flat, stress-free, glass plate to a shallow spherical surface.

2.1 Basic Equations

The following equations were obtained by Von Kármán (1910) and subsequently have been extensively used (Szilard (1974)) for the analysis of the coupled bending and stretching effects in an initially flat, homogeneous, isotropic plate:

$$-Ehc^2\Delta\Delta w + F(\Phi,w) = -p \qquad (2.1.1)$$

$$\tfrac{1}{2}EhF(w,w) + \Delta\Delta\Phi = 0 \qquad (2.1.2)$$

In these equations, F is the differential operator, which for rectangular cartesian coordinates x,y, is in the form

$$F(w,\Phi) = w_{,xx}\,\Phi_{,yy} - 2w_{,xy}\,\Phi_{,xy} + w_{,yy}\,\Phi_{,xx} \qquad (2.1.3)$$

Δ is the laplacian

$$\Delta w = w_{,xx} + w_{,yy}$$

w is the normal displacement from which the bending stress resultants can be calculated

$$\begin{aligned} M_x &= -Ehc^2\,(w_{,xx} + \nu w_{,yy}) \\ M_y &= -Ehc^2\,(w_{,yy} + \nu w_{,xx}) \\ M_{xy} &= -Ehc^2\,(1-\nu)\,w_{,xy} \end{aligned} \qquad (2.1.4)$$

and Φ is the Airy stress function from which the membrane stress resultants can be calculated

$$\begin{aligned} N_x &= \Phi_{,yy} \\ N_y &= \Phi_{,xx} \\ N_{xy} &= -\Phi_{,xy} \end{aligned} \qquad (2.1.5)$$

These equations are valid when the strains and the square of the rotations $w_{,x}$ and $w_{,y}$ are small in comparison with unity. Since glass fails at a fairly small strain (10^{-3}), these equations will be very accurate for the bending of a glass plate to a shallow, curved surface. The tangential tractions on the plate surface are assumed to be zero. The bending stress at the surface on the side of the positive normal is

$$\sigma_{Bx} = 6M_x/h^2, \text{ etc.} \tag{2.1.6}$$

while the membrane (direct) stress is

$$\sigma_{Dx} = N_x/h \quad , \text{etc} \tag{2.1.7}$$

The shallow spherical mold is at the distance normal to the initial plane of the plate given by

$$w_0 = (x^2 + y^2)/2R \tag{2.1.8}$$

So in a region of the plate which is in contact with the (rigid) mold, $w = w_0$ which gives the bending stress (2.1.4, 2.1.8)

$$\sigma_{Bx} = \sigma_{By} = \sigma_{B0} = Eh/2(1-\nu)R \tag{2.1.9}$$

and (2.1.2) simplifies to

$$\Delta\Delta\Phi = -Eh/R^2 \tag{2.1.10}$$

while (2.1.1) gives the pressure acting on the plate in the contact region

$$p_0 = -\frac{1}{R}\Delta\Phi \tag{2.1.11}$$

Thus the equations are linear in the contact region (2.1.10), but nonlinear elsewhere (2.1.1, 2.1.2). However, a satisfactory procedure is to ignore the membrane coupling term in (2.1.1) and solve the standard equation for bending

$$- Ehc^2 \Delta\Delta\tilde{w} = -p \qquad (2.1.12)$$

and then compute the resulting membrane stresses from (2.1.2)

$$\Delta\Delta\tilde{\Phi} = -\tfrac{1}{2}EhF(\tilde{w},\tilde{w}) \qquad (2.1.13)$$

This provides an accurate solution if the membrane stress is small, i.e. if

$$|F(\tilde{\Phi},\tilde{w})| << Ehc^2|\Delta\Delta\tilde{w}| \qquad (2.1.14)$$

Generally the induced membrane stress will provide a stiffening effect which reduces the bending stress for a given pressure loading. Thus $\tilde{w}$ should give a conservative estimate of the bending stress.

In the E-Systems fabrication procedure (Perry, 1980) the finished panel consists of a sandwich with a honeycomb core, the glass mirror on one side, and a slotted steel plate on the other. The honeycomb core is first molded to the spherical shape and cured. Then the glass mirror, with adhesive on one surface, is placed between the mold and the honeycomb, as shown in Fig. 2.1. A wood frame is placed around the sides and then everything is enclosed by a vacuum bag. As the vacuum p is increased, a region of contact developes at the plate center and regions of contact with the honeycomb develop at the edges.

2.2 Circular Plate

Some features of the stresses during partial contact can be obtained by considering the circular plate. Axisymmetry reduces this to a one dimensional problem, and the uniform circle of contact with the honeycomb at the edges avoids any large transverse shear stress as the loading is initiated (Fig. 2.1).

The loading of the plate consists of the axial force $\pi b^2 p$ applied at the center through the mold and at the edge through the honeycomb.

In the contact region of radius a, the plate conforms to the mold

$$w = r^2/2R \qquad \text{for } 0 \leq r \leq a \tag{2.2.1}$$

while in the free region, the solution of (2.1.12) (with $p \equiv 0$) is

$$\tilde{w} = \frac{b^4 p}{8Ehc^2}\left[(C_1+\rho^2)\log\rho + C_2 + C_3\,\rho^2\right] \qquad \text{for } \rho_c \leq \rho \leq 1 \tag{2.2.2}$$

in which

$$\rho = r/b$$
$$\rho_c = a/b$$

The condition of zero bending moment at the edge in contact with the honeycomb gives the condition

$$3 + \nu - C_1(1-\nu) + 2C_3(1+\nu) = 0 \tag{2.2.3}$$

The conditions on continuity of slope and curvature at the contact point r = a combine into the condition

$$\frac{d^2w}{dr^2} - \frac{1}{r}\frac{dw}{dr} = 0 \tag{2.2.4}$$

which immediately gives

$$C_1 = \rho_c^{\,2} \tag{2.2.5}$$

Then the condition of continuity of slope yields the relation between pressure and contact zone radius

$$\frac{pb^2R}{Eh^3} = \frac{2}{3(1-\nu)}\left[(1-\nu)(1-\rho_c^{\,2})+2(1+\nu)\log\rho_c^{-1}\right]^{-1} \tag{2.2.6}$$

the curve of which is shown in Fig. 2.1 for $\nu = 0.3$. As $\rho_c \to 1$ for full contact, the result (2.2.6) indicates that infinite pressure would be required

$$\frac{pb^2R}{Eh^3} \cong \left[6(1-\nu)(1-\rho_c)\right]^{-1} \qquad \text{for } 0.5 \lesssim \rho_c < 1 \qquad (2.2.7)$$

This solution neglects the effects of transverse shear deformation and stretching of the normal of the plate as well as the compliance of the mold and honeycomb. Nevertheless, the behavior shown in Fig.2.1 is correct, that a very high pressure is required for full deformation of the plate to a spherical surface. Normally, in practice, a small region near the edge will remain which is not of the correct curvature.

It may be verified that the slope $d\tilde{w}/dr$ of the displacement (2.2.2) remains less than that of the honeycomb at the outer edge r=b. Thus the contact remains on a line. Furthermore it may be verified that the maximum bending stress occurs at the contact point r=a, where it equals that in the central contact region (2.1.9)

$$\sigma_B = \sigma_{B0} = Eh/2(1-\nu)R \qquad (2.2.8)$$

We conclude that for the circular plate there is no overshoot of stress during fabrication; the residual stress at full contact is the most severe.

2.3 Square Plate - Corner Effects

In contrast to the circular plate, more care must be exercised in forming the rectangular plate to a spherical surface, since the corners are particularly vulnerable. If a male mold is used and the plate loaded by uniform pressure, no problem occurs. When a female mold is used, as in the E-Systems fabrication procedure (Perry, 1980), only the tips of the plate corners are initially in contact. As

indicated in Fig. 2.2, at the early increments of loading, whether by uniform pressure or by a male mold, the area of contact at the corner is small so the transverse shearing stress is high. As the loading increases, the contact area increases and the shear stress would be expected to decrease.

For an approximate solution which will give the correct behavior at the corners, the plate will be treated as two uncoupled beams with fibers in the x and y directions shown in Fig. 2.2. Each will be loaded by pressure. Because of the symmetry, the two will have the same deflection. The coupling of the x and y behavior which is being ignored should be negligible in the corner regions.

2.3.1 - Beam Solution - The basic equations of elementary (Euler-Bernoulli) beam theory are

$$\frac{dQ}{dx} = -q \qquad (2.3.1)$$

$$\frac{dM}{dx} = Q$$

$$\frac{d\beta}{dx} = \frac{M}{EI}$$

$$\frac{dw}{dx} = -\beta$$

where Q is the transverse shear resultant, M the moment resultant, and β the rotation.

For the beam of Fig. 2.2, the width is

$$\eta = 2^{3/2}L(1-\rho) \qquad (2.3.2)$$

$$\rho = x/2^{1/2}L$$

so that the load per unit length is

$$q = -p\eta \tag{2.3.3}$$

and the cross-sectional moment of inertia is

$$I = \eta h^3/12 \tag{2.3.4}$$

For sufficiently high pressure the beam will contact the honeycomb surface in a region near the ends $\rho_c \leq \rho \leq 1$. If the preformed honeycomb is assumed to be rigid in comparison with the glass plate, then the displacement, rotation and moment in the contact zone are

$$\begin{aligned} w &= x^2/2R + \text{const.} \\ \beta &= -x/R \\ M &= -EI/R \qquad \text{for } x_c \leq x \leq 2^{\frac{1}{2}}L \\ &\qquad\qquad (\text{i.e.} \rho_c \leq \rho \leq 1) \end{aligned} \tag{2.3.5}$$

In the portion of the beam not in contact, the pressure loading is prescribed. By symmetry the shear Q and rotation β must be zero at the center x=0. The integrations (2.3.1) give

$$\begin{aligned} Q &= p2L^2 (2\rho - \rho^2) \\ M &= -pL^2\eta (2+2\rho-\rho^2)/3 + m \\ \beta &= -[4\cdot 2^{\frac{1}{2}} pL^3 \rho(2+\rho-\rho^2/3) \\ &\quad -6m \log (1-\rho)^{-1}]/Eh^3 \\ &\qquad\qquad \text{for } 0 \leq \rho \leq \rho_c \end{aligned} \tag{2.3.6}$$

The constant m gives the additional moment in the beam due to the contact region. For m=0, the solution (2.3.6) is exactly that for uniform pressure and concentrated point loads at the ends.

The rotation β and moment M from (2.3.5) and (2.3.6) must be continuous at the point $\rho=\rho_c$. Equating the moments gives the unknown

moment in terms of the pressure and contact point

$$m = (n[pL^2(2+2\rho-\rho^2)/3-Eh^3/12R])_{\rho=\rho_c} \tag{2.3.7}$$

then equating the rotations gives the relation between pressure and

$$pL^2R/Eh^3 = (3/32)\ G(\rho_c) \tag{2.3.8}$$

where

$$G(\rho) = \frac{8}{3}\ \frac{1 - (1-\rho)(1+\log(1-\rho)^{-1})}{\rho(2+\rho-\rho^2/3)-(1-\rho)(2+2\rho-\rho^2)\log(1-\rho)^{-1}}$$

This is shown as Solution EB in Fig. 2.3. Including the bending in the y-direction, the total pressure is twice that of (2.3.8). The limiting values for small and large contact regions are

$$G(\rho_c) \sim \begin{cases} 1 & \text{for } \rho_c \to 1 \\ 2/3\rho_c & \text{for } \rho_c \to 0 \quad \text{(complete contact)} \end{cases} \tag{2.3.9}$$

Similar to the solution for a circular plate on a male mold (Fig. 2.1), this beam solution indicates that infinite pressure is required to produce complete contact with the mold. In contrast with Fig. 2.1, which shows the central contact zone increasing from zero pressure, this corner solution (Solution EB in Fig. 2.3) indicates contact only at the very tip until a finite pressure is reached. Such a solution is not realistic, since a finite force at the tip corresponds to infinite transverse shear stresses. The appropriate correction will be considered in the following Section 2.3.2

The bending stress distribution in the free region is from (2.3.6)

$$\sigma_B = -6M/h^2$$
$$= (2pL^2/h^2)[3-(1-\rho)^2 - 2\gamma/(1-\rho)] \tag{2.3.10}$$

$$\gamma = 3m/2^{5/2}pL^3$$

$$= \frac{1}{2}(1-\rho_c)[3-(1-\rho_c)^2 - 8/3G(\rho_c)]$$

This has a maximum value for a given pressure at the point ρ given by

$$1-\rho = \gamma^{1/3} \qquad (2.3.11)$$
$$(0 < \rho < \rho_c)$$

Substituting (2.3.11) into (2.3.10) gives the maximum value

$$(\sigma_B)_{max} = (Eh/2R)\ 9G(\rho_c)(1-\gamma^{2/3})/8 \qquad (2.3.12)$$

which is shown as Solution EB in Fig. 2.4. The most severe bending stress occurs when the pressure has just reached the value to initiate spreading of the contact zone, i.e., at

$$\rho_c = 1 \qquad (2.3.13)$$

$$p_{Total}\ L^2R/Eh^3 = 3/16$$

$$\gamma = 0$$

$$\sigma_B = (Eh/2R)\ 9/8$$

Thus the bending stress near the corner during fabrication exceeds that of full contact by only the factor 9/8. Since the preceding solution for the circular plate gave no excess of the full contact stress, we conclude that bending stress in the plate during fabrication is not a problem.

2.3.2 - Shear Deformation Solution - To include the effects of transverse shear deformation only the last equation of the set (2.3.1) is modified

$$\frac{dw}{dx} = -\beta + \mu Q/Ehn \qquad (2.3.14)$$

in which E/μ is the equivalent transverse shear modulus. For an isotropic plate, $\mu = 3.12$. The results for the free region (2.3.6) are unchanged. In the contact region, the equations are combined to give

$$\frac{d}{dx}\left(EI\,\frac{d\beta}{dx}\right) = Q = \frac{Eh\eta}{\mu}\left(\frac{dw}{dx} + \beta\right) \tag{2.3.15}$$

Since the normal displacement w is known, this is a second order differential equation for the rotation of the normal β, which simplifies when

$$z = \eta/h(\mu/3)^{\frac{1}{2}} \tag{2.3.16}$$

is used as the independent variable and when Eh is constant to the form

$$\frac{1}{z}\,\frac{d}{dz}\left(z\,\frac{d\beta}{dz}\right) - \beta = \frac{dw}{dx} \tag{2.3.17}$$

The complementary solutions are Bessel functions of the second kind. If $dw/d\eta$ is constant, the solution which gives zero stress resultants at the tip (z=0) is

$$\beta = -\frac{dw}{dx} + C\,I_0(z) \tag{2.3.18}$$

in which C is an arbitrary constant.

The particular solution is exact when the slope dw/dx is constant and a very good approximation when the slope does not change substantially in a distance equal to the thickness h.

The shear and moment in the contact region are

$$Q = (Eh/\mu)\,\eta\,C\,I_0(z) \tag{2.3.19}$$

$$M = \frac{Eh^3}{12}\,\eta\left[\frac{dz}{dx}\,C\,I'_0(z) - \frac{1}{R}\right]$$

The constant C does not appear in the Euler-Bernoulli beam solution and can be used to obtain continuity of transverse shear Q between

the free and contact areas. Thus at the contact point $\rho=\rho_c$ we obtain

$$C\ I_0(z) = \frac{2pL^2\mu}{Eh\eta}\ (2\rho-\rho^2) \qquad (2.3.20)$$

and for continuity of moment

$$m = \left(\eta\left[pL^2\left\{(2+2\rho-\rho^2)/3-\rho(2-\rho)I'_0(z)/zI_0(z)\right\} - Eh^3/12R\right]\right)_{\rho=\rho_c} \qquad (2.3.21)$$

which is similar to (2.3.7), and for continuity of rotation

$$pL^2R/Eh^3 = (3/32)\ G_{SD}\ (\rho_c) \qquad (2.3.22)$$

in which the corrected form of (2.3.8) is

$$G_{SD}(\rho) = \frac{8}{3}\left[1-(1-\rho)(1+\log(1-\rho)^{-1})\right] \qquad (2.3.23)$$
$$\div\left\{\rho(2+\rho-\rho^2/3)+(1-\rho)\left[3\rho(2-\rho)z^{-2} - \left(2+2\rho-\rho^2-3\rho(2-\rho)\ I'_0(z)/zI_0(z)\right)\log(1-\rho)^{-1}\right]\right\}$$

For small contact area, the limit is

$$G_{SD}(\rho) \to 8\ z^2/9(1-\rho) \qquad \text{for } \rho \to 1 \qquad (2.3.24)$$

The previous equations (2.3.10-12) remain valid, but with the correction to γ

$$\gamma = \left\{\frac{1}{2}\ (1-\rho)\left[3-(1-\rho)^2 - 8/3\ G_{SD}(\rho) - 3\rho(2-\rho)\ I'_0(z)/z\ I_0(z)\right]\right\}_{\rho=\rho_c} \qquad (2.3.25)$$

This gives the curves for maximum bending stress as a function of contact area shown in Fig. 2.4 for various values of L/h. The conclusion remains that the bending stress during fabrication does not exceed significantly that of full contact.

In contrast, the transverse shear stress is very large at the first incidence of loading. From (2.3.19, 20, 22) the shear stress at the edge of the contact zone, where it has its maximum value, is

$$\sigma_{shear} = Q/h\eta = (Eh/2R)\left[3h\, G(\rho)(2\rho-\rho^2)/32\eta\right]_{\rho=\rho_c} \qquad (2.3.26)$$

The limit,for very small pressure and contact area,of the ratio of shear stress to full contact bending stress is

$$\sigma_{shear}/(Eh/2R) = 2^{3/2}L/\mu h \qquad \text{for } \rho_c \to 1 \quad (2.3.27)$$

For a thin plate L/h is very large. The conclusion is that the use of a rigid female mold for a rectangular plate is hazardeous.

Including the flexibility of the female mold (honeycomb) reduces (2.3.27) by the factor

$$1 + (Eh/\mu)_{Plate} \,/\, (Eh/\mu)_{Honeycomb} \qquad (2.3.28)$$

Even with this reduction, the shear stress remains excessively large. However, E-Systems has encountered only slight difficulty in that a few percent of the panel corners have been broken during fabrication. There are several reasons for this not being a serious problem:

1) The honeycomb cell size (1/2 in) is sufficient to distribute a "point" corner contact. From Fig. 2.5 when the contact length is one plate thickness, the shear stress is reduced to about the full contact bending stress magnitude.

2) The high stress occurs only at very low pressure; during

actual fabrication the rate of pressurization could induce transients and avoid any corner failure.

3) Small internal cracks at the corner caused by transverse shear stress, within one thickness, may not be significant for the function of the reflector.

We conclude that if the panel survives the initial loading during fabrication, then the most severe stresses occur at full contact when the membrane stresses will be maximum and added to the full contact bending stresses.

3.0 RESIDUAL STRESS

In this Section the stress is computed which exists when the originally flat glass plate is fully deformed to the spherical surface. The equations are simpler for this problem, since the normal displacement is known everywhere (2.1.8), which gives the bending stress (2.1.9) at every point in the plate except for a narrow zone near the free edges. The induced membrane stress requires the solution of the familiar partial differential equation (2.1.10). Only normal pressure is assumed to act on the plate, since tangential friction forces of the mold surface should be negligible. The condition of zero tractions on the plate edge is satisfied if Φ and its normal derivative are zero along the edge, which provides a standard, well-posed problem. After the calculation of Φ the pressure distribution is obtained from (2.1.11), which is the pressure necessary to hold the plate in the deformed configuration. After curing and removal of the complete panel from the mold, if the springback deformation is small, then the pressure (2.1.11) becomes the normal stress in the layer of adhesive between glass panel and honeycomb. The simple, closed-form solutions for the circular plate and for the long rectangular strip plate will be discussed first, followed by the numerical (finite difference) solutions for square and rectangular plates.

3.1 Circular Plate

The axisymmetric problem is straightforward. The solution of (2.1.10) which satisfies the condition of zero tractions on the edge at $\rho = r/b = 1$ is

$$\Phi = - \frac{Ehb^4}{64R^2} (1 - \rho^2)^2 \qquad (3.1.1)$$

Transforming (2.1.6,8) into polar coordinates provides the stress components in the radial and circumferential directions.

$$\sigma_{Dr} = \Phi_{,r}/r = \sigma_{DO}\ (1-\rho^2)/2 \qquad (3.1.2)$$

$$\sigma_{D\theta} = \Phi_{,rr} = \sigma_{DO}(1-3\rho^2)/2$$

while the pressure from (2.1.11) is

$$p = -(h/R)(\sigma_r+\sigma_\theta) = -(\sigma_{DO}\ h/R)(1-2\rho^2) \qquad (3.1.3)$$

The maximum magnitude of membrane stress for this circular plate, which will be used for the reference membrane stress, is

$$\sigma_{DO} = Eb^2/8R^2 \qquad (3.1.4)$$

The distributions (3.1.2,3) are shown in Fig. 3.1. Note that the radial stress is always tensile, while the circumferential stress is tensile in the center $0 \leq \rho < 0.58$, but compressive in the annulus $0.58 < \rho \leq 1$. Any tensile stress is, of course, undesirable in glass. The tensile membrane stress in the center undoubtedly contributes to the cracking of some of the panels fabricated by E-Systems. However, the compressive circumferential stress at the edge is beneficial, particularly since the main crack-initiating flaws may be at the edge.

3.2 Rectangular Plate

The square and rectangular plates are of the greatest practical interest, since they can be fit together more readily to form the large spherical surface necessary for significant power generation.

3.2.1 - High Aspect Ratio - For a long plate strip with a high value of the ratio of length to width $Ly/L \gg 1$, the solution of (2.1.10) is independent of the length coordinate y, except near the ends, and is easily found to be

$$\Phi = -\frac{EhL^4}{24R^2}\ (1-\rho^2)^2 \qquad (3.2.1)$$

in which L is the half width and

$$\rho = x/L$$

The stress components (2.1.6, 8) are

$$\sigma_{Dy} = \sigma_{DO}\, 4(1-3\rho^2)/3 \qquad (3.2.2)$$

$$\sigma_{Dx} = \sigma_{Dxy} = 0$$

where the radius b is replaced by the half-width L in the reference stress (3.1.4)

$$\sigma_{DO} = EL^2/8R^2 \qquad (3.2.3)$$

The pressure (2.1.11) is

$$p = -\sigma_{Dy}\, h/R \qquad (3.2.4)$$

The stress (3.2.2) is larger than that in an inscribed (b=L) circular plate (3.1.2) but has the same feature of tensile stress in the central portion and compressive stress near the edge in the direction parallel to the edge.

3.2.2 - Moderate Aspect Ratio - For the square plate and plates with moderate aspect ratios, simple closed form solutions of (2.1.10), with the boundary condition of zero Φ and its normal derivative, are not possible. Therefore, a finite difference solution based on the standard thirteen point, central difference stencil discussed by Szilard (1974) was obtained. Mesh convergence studies and comparison with published solutions for the analogous problem of the bending of a flat plate clamped on all edges and loaded by pressure showed the error to be less than one percent.

The results for the stresses on the axes of symmetry, which are the largest stresses, are shown in Figs. 3.2 - 3.5 for length to width

ratios Ly/L = 2.0, 1.5, 1.3, 1.0. For Ly/L = 2, the distribution of stress σ_{Dy} at the center across the width (at y = 0) is very close to that for the infinite strip (3.2.2) shown by the dashed line in Fig. 3.2 The maximum tensile stress occurs at the plate center, while the maximum compressive stress occurs at the center of the longer edge. The variation in these peak stresses with aspect ratio is shown in Fig. 3.6. The validity of the plate strip solution (3.2.2) for $Ly/L \geq 2$ is clear. Also of interest is that the stress in the center of the square plate is close to that of the inscribed circular plate, and that the circumscribed circular plate gives an upper bound on the stress in the rectangular plate.

3.3 Stress in Adhesive

The pressure computed from (2.1.11) which is given by (3.1.3) for the circular plate and by (3.2.4) for the plate strip, is necessary to hold the initially flat plate in the curved configuration. As indicated in Fig. 3.1 for the circular plate, this normal pressure is of one sign in the center region, which corresponds to a positive pressure between the male mold and the plate, and of opposite sign in the outer region $0.58 \leq r/b \leq 1$, which corresponds to positive pressure between the female mold (the honeycomb) and the plate. The total resultant of pressure acting on the plate must, of course, be zero, since the plate is in static equilibrium.

The curved, composite panel, consisting of the glass plate, honeycomb core and steel back plate, has a much higher bending stiffness than the glass plate alone. Thus, when the panel is removed from the mold relatively little change in the curvature of the glass occurs, which means that the positive pressure of the male mold is replaced by tensile stress in the adhesive between glass and honeycomb. From Fig. 3.1 the adhesive in the central region of the circular plate $0 \leq r/b \leq 0.57$ is in tension with the maximum at the center

$$(\sigma)_{\substack{\text{Adhesive} \\ \max}} = h\sigma_{DO}/R = Ehb^2/8R^3 \qquad (3.2.5)$$

The numerical results for rectangular plates of aspect ratios Ly/L = 2.0, 1.5, 1.0 are shown in Figs. 3.7 - 3.9, respectively. Similar to the circular plate, the rectangular plate has the central region of tension in the adhesive, leaving a strip of compression of about equal width at the ends and sides. The corners are regions of low compressive stress. The variation of the maximum tension at the center with aspect ratio is shown in Fig. 3.10. The square plate exceeds that of the inscribed circular plate by only 13%.

3.4 Bending Stress - Edge Effect

In addition to the membrane stresses, the deformation of the initially flat plate to the shallow, spherical surface (2.1.8) causes the bending stress (2.1.9). This stress is uniform everywhere in the plate. However, in the mold the edges are free from any significant stress. This is a contradiction which cannot be resolved with elementary theory, nor with shear deformation theory. Both shear deformation and stretching of the normal must be considered.

We wish to subtract the bending stress (2.1.9) from the free edges, while holding the plate in contact with the mold (2.1.8) only with pressure normal to the surface. The effect is localized to the edge, so that the curvature of the plate is negligible as is the variation along the edge. The equations are similar to those for the beam (2.3.1) with shear deformation (2.3.14)

$$\frac{dQ}{dx} = - p \qquad (3.4.1)$$

$$\frac{dM}{dx} = Q$$

$$\frac{d\beta}{dx} = M/Ehc^2$$

$$\frac{dw}{dx} = - \beta+\mu Q/Eh$$

in which the resultants are per unit width, x is the distance from the edge, and w is the normal displacement of the midsurface. What is new is the condition that the face is constrained to have zero normal displacement, which gives the relation

$$p = (8/3h(1-\nu^2))\ [-Ew+\nu(1+\nu)3M/2h] \tag{3.4.2}$$

The system (3.4.1, 3.4.2) is of the fourth order and can be reduced to these coupled, second order equations for the displacement w and rotation β

$$\frac{d^2w}{dx^2} - \frac{8\mu}{3(1-\nu^2)h^2}\, w + \left[1 + \frac{4\mu\nu}{(1-\nu)12(1-\nu^2)}\right] \frac{d\beta}{dx} = 0$$

$$-\frac{dw}{dx} + \mu c^2 \frac{d^2\beta}{dx^2} - \beta = 0 \tag{3.4.3}$$

The solutions are of the form

$$w = hA\ e^{-\lambda x/h} \tag{3.4.4}$$

$$\beta = B\ e^{-\lambda x/h}$$

in which A and B are constants. Substitution into (3.4.3) gives

$$\begin{bmatrix} \lambda^2 - \dfrac{8\mu}{3(1-\nu^2)} & -\lambda\left(1 + \dfrac{4\mu\nu}{12(1-\nu^2)(1-\nu)}\right) \\ \lambda & \dfrac{\mu\lambda^2}{12(1-\nu^2)} - 1 \end{bmatrix} \begin{bmatrix} A \\ B \end{bmatrix} = 0 \tag{3.4.5}$$

For a nonzero solution the determinant must be zero, which gives the polynominal for λ

$$\lambda^4 - 2b\lambda^2 + 32 = 0 \tag{3.4.6}$$

in which

$$b = \frac{4\mu}{3(1-\nu^2)}\left[1 - \frac{3\nu(1+\nu)}{2\mu}\right]$$

The first quadrant root of (3.4.6) is

$$\lambda = 2^{5/4}\, e^{i\phi} \tag{3.4.7}$$

in which

$$2\phi = \cos^{-1}\,(b/2^{5/2})$$

For the isotropic material $\mu = 3.12$ and for $\nu = 0.3$, we obtain

$$\phi = 24.4^0 \tag{3.4.8}$$

The real and imaginary parts of (3.4.4) are the linearly independent solutions of (3.4.3) which decrease for $x \to \infty$.

The solution which satisfies the conditions of a prescribed moment and zero shear at the edge

$$\sigma_B = 6M/h^2 = -\sigma_{BO} \qquad \text{at } x = 0$$

$$Q = 0 \tag{3.4.9}$$

is the following

$$\sigma_B/\sigma_{BO} = -e^{-\zeta\cos\phi}\sin(\zeta\sin\phi+\phi)/\sin\phi$$

$$\sigma_{xz}/h\sigma_{BO} = Q/h\sigma_{BO} = -(2^{5/4}/6)e^{-\zeta\cos\phi}\sin(\zeta\sin\phi)/\sin\phi$$

$$p/\sigma_{BO} = -(2^{5/2}/6)e^{-\zeta\cos\phi}\sin(\zeta\sin\phi-\phi)/\sin\phi \tag{3.4.10}$$

in which

$$\zeta = 2^{5/4}\, x/h$$

Adding the uniform bending stress (2.1.9) to (3.4.9) gives the curves for the stresses shown in Fig. 3.11. The interpretation is that the bending stress equals (2.1.9) everywhere in the panel except in a zone of width equal to about two plate thicknesses. The elementary theory requires that a moment resultant be supplied at the edge; the present more detailed analysis shows how the moment at the edge is replaced by a normal pressure distribution near the edge with the proper resultant moment. As seen from the curve in Fig. 3.11, there occurs a high compressive stress in the honeycomb surface and, beginning at about one-half a thickness from the edge, a compressive stress on the mold surface.

Of significance is that no overshoot in the bending stress in the glass plate occurs, and that the transverse shear stress is small. Note that this very localized normal pressure can be much larger than the pressure due to the membrane stresses (i.e. in Fig. 3.10). A severe demand is placed on the honeycomb, to support the large localized edge compression

$$p = - 0.94 \, \sigma_{BO} \tag{3.4.11}$$

and on the adhesive, after removal of the panel from the mold, to support the large tensile stress

$$p = 0.14 \, \sigma_{BO} \tag{3.4.12}$$

Otherwise the glass surface will not retain the spherical curvature in this edge region.

4.0 SPRINGBACK DEFORMATION

The membrane and bending stresses in the initially flat plate deformed to a spherical surface were discussed in the preceding Section 3. These stresses remain as the residual stresses if the deviation from the spherical shape, which occurs when the cured panel is removed from the mold, is not large. In this Section this springback deflection is quantified. Naturally, the final deviation of the panel from the spherical surface is an important parameter for the system.

The total normal displacement of the glass plate from the initial flat surface is

$$w = w_0 + w_1 \tag{4.0.1}$$

where w_0 is the nominal shallow spherical surface (2.1.8) and w_1 is the springback deviation. During the forming, the stiffness of the glass plate is of primary concern (2.1.1, 2). For the springback of the cured composite panel, the much larger effective bending stiffness D of the sandwich is the governing factor. If the honeycomb thickness H is large in comparison to the glass plate thickness h and the backplate thickness h_s, then the effective bending stiffness is

$$D \cong H^2/(1-\nu^2)\left((Eh)^{-1}+(E_s h_s)^{-1}\right) \tag{4.0.2}$$

If the backplate has the same effective stiffness as the glass

$$E_s h_s \cong Eh \tag{4.0.3}$$

then

$$D \cong Eh\, H^2/2\,(1-\nu^2) \tag{4.0.4}$$

The panel does have curvature, but the curvature will be negligible in the springback if the parameter Λ, defined by

$$\Lambda = b/R^{\frac{1}{2}} \left(D/(Eh + E_s h_s)\right)^{\frac{1}{4}} \qquad (4.0.5)$$

$$\cong b/ (HR/2)^{\frac{1}{2}}$$

where b is a characteristic radius, is not large. If Λ is large, then significant bending effects occur only in zones near the edges (Reissner, 1956) and the main springback deformation will be governed by the membrane stiffness of the panel, which is negligibly affected by the honeycomb core. Therefore, for an effective utilization of the sandwich panel concept, the honeycomb core thickness H must be large enough so that

$$\Lambda \lesssim 1 \qquad (4.0.6)$$

In this case, the springback deformation is just plate bending

$$D \, \Delta\Delta \, w_1 = - \, p \qquad (4.0.7)$$

in which the pressure distribution is the negative of that required to hold the glass plate in the spherical curvature, as computed in Section 3.

If the honeycomb core and the backplate are not preformed, then the load p is increased accordingly. In the E-Systems fabrication procedure (Perry, 1980), the honeycomb is preformed and the steel backplate cut to reduce the pressure required for the forming. The cuts are filled with epoxy, however, so that in the cured condition, the steel backplate should have nearly full strength. For the present analysis, the backplate is assumed to offer no resistance to forming and to be at full strength to resist springback. Then the pressure p in (4.0.7) is only that required to deform the glass and the panel bending stiffness is (4.0.2). The edges are free of shear, but are subject to the negative of the moment resultant of the nominal bending stress (2.1.9)

$$(M)_{edge} = h^2 \, \sigma_{BO}/6 \qquad (4.0.8)$$

$$= Eh^3/12(1-\nu)R$$

The springback of the cured panel due to this edge bending is easily obtained for the rectangular panel

$$w_{B1} = (x^2 + y^2)\, Ehc^2/2\, DR \tag{4.0.9}$$

The corner displacement is

$$(w_{B1})_c = L^2 Ehc^2/DR \tag{4.0.10}$$

which for (4.0.3) is

$$(w_{B1})_c = L^2 h^2/RH^2 6(1-\nu^2) \tag{4.0.11}$$

4.1 Circular Panel

For the circular panel of radius b, the pressure is given by (3.1.3) and the solution to (4.0.7), which satisfies the free edge condition of zero moment and zero transverse shear, is

$$w_1 = \frac{b^4}{64D}\,(\sigma_{DO}\, h/R)\left[\rho^4 - \frac{2}{9}\rho^6 - \frac{4}{3}\,\frac{2+\nu}{1+\nu}\,\rho^2\right] \tag{4.1.1}$$

Since an arbitrary rigid body displacement can be added, the displacement at the center is chosen to be zero. The edge displacement is then

$$(w_1)_{edge} = -\frac{b^4}{64D}\,(\sigma_{DO}\, h/R)\,(17+5\nu)/9(1+\nu) \tag{4.1.2}$$

which for $\nu = 0.3$ and equal stiffness backplate (4.0.3) reduces to

$$(w_1)_{edge} = -\,0.00562\, b^6/H^2R^3 \tag{4.1.3}$$

The springback deflection curve (4.1.1) is shown in Fig. 3.1.

The change in slope is of greatest interest

$$\beta_1 = -\frac{dw_1}{dr} = \beta_{10}\left[-(3\rho^3-\rho^5)(1+\nu)/2 + (2+\nu)\rho\right] \qquad (4.1.4)$$

which has the edge value, which will be used as the reference,

$$\beta_{10} = (\beta_1)_{edge} = \frac{b^3}{24D(1+\nu)}\frac{\sigma_{D0}h}{R} \qquad (4.1.5)$$

For (4.0.3) and $\nu = 0.3$ this gives

$$\beta_{10} = 0.00729\ b^5/H^2R^3 \qquad (4.1.6)$$

and in terms of the edge rotation, the edge displacement (4.1.3) is

$$(w_1)_{edge} = -0.771\ \beta_{10}\ b \qquad (4.1.7)$$

4.2 Rectangular Panel

The springback deflection for the center portion of the high aspect ratio panel $L_y/L \gtrsim 2$ can be obtained in closed form. The pressure distribution (3.2.4) used in (4.0.7) has the solution

$$w_1 = -\frac{8L^4}{45D}\frac{\sigma_{D0}h}{R}\ \frac{15\rho^2 - 5\rho^4 + \rho^6}{16} \qquad (4.2.1)$$

$$\beta_1 = -\frac{dw_1}{dx} = \frac{8L^3}{45D}\frac{\sigma_{D0}h}{R}\ \frac{15\rho-10\rho^3 + 3\rho^5}{8}$$

in which $\rho = x/L$. The edge values for (4.0.3) and $\nu = 0.3$ are substantially larger than for the circular panel

$$(w_1)_{edge} = -3.81\ \beta_{10}\ L \qquad (4.2.2)$$

$$(\beta_1)_{edge} = 5.55\,\beta_{10} \tag{4.2.3}$$

in which β_{10} is the edge springback rotation for the inscribed circular panel (4.1.5, 6) with b = L.

The numerical results for the square panel with the self-equilibrating pressure distribution shown in Fig. 3.9 and with free edges have been obtained. In Fig. 4.1 is shown the springback displacement along the x-axis from the panel center to the middle of the edge, which is only slightly larger than that for the inscribed circular plate. Also shown in Fig. 4.1 is the displacement along a line from the panel center to the corner which is somewhat larger. The contours of constant displacement are shown in Fig. 4.2. Except near the corner, the pattern is close to the axisymmetric circular plate in Fig. 3.1. The contours of constant springback of the angle of the normal are shown in Fig. 4.3. The corner value is

$$(\beta_1)_c = 2.44\ \beta_{10} = 1.01^o\ (L^5/R^3H^2) \tag{4.2.4}$$

4.3 Viscoelastic Core

The springback deflection from (4.0.7), obtained for the circular panel (4.1.1), the strip panel (4.2.1) and for the square panel (Figs. 4.1, 4.2), is the instantaneous elastic response of the glass and steel plates neglecting the transverse shear deformation of the honeycomb core. The experience of E-Systems (Perry, 1980) is that the springback deflection continues to increase for about four days after removal of the panel from the mold. It seems likely that this is due to a viscoelastic behavior of the adhesive and the epoxy used to stiffen the honeycomb. Since this affects primarily the transverse shear stiffness, the effect can be analyzed by considering shear deformation only.

For the pure shear deformation of a rectangular panel, the transverse shear components are related to the slopes

$$Q_x = GH\,w_{,x} \tag{4.3.1}$$
$$Q_y = GH\,w_{,y}$$

in which G is the effective shear modulus of the

panel and H is the thickness. The equation for equilibrium is

$$Q_{x,x} + Q_{y,y} = - p \tag{4.3.2}$$

or using (4.3.1)

$$GH \Delta W_{1SD} = - p \tag{4.3.3}$$

However, the pressure distribution for the springback is the negative of (2.1.11). Thus the solution of (4.3.3) is simple

$$W_{1SD} = - \Phi/GHR + \text{const.} \tag{4.3.4}$$

where Φ, the solution of (2.1.10), is the stress function whose derivatives (2.1.5) give the residual membrane stress in the glass face plate. The normal derivative of Φ is zero on the edge; thus (4.3.4) satisfies the condition of zero transverse shear (4.3.1) on the edge. A peculiar consequence is that Φ is zero on the edge, so that the springback displacement (4.3.4) due to the shear deformation is constant on the edge. The larger displacement of the corner Figs. 4.1, 4.2 seems to be an instantaneous elastic effect only.

Using (3.1.1) in (4.3.4) gives the springback deflection of the circular panel due to transverse shear deformation

$$W_{1SD} = \beta_{10}\gamma(b/4) \left[(1-\rho^2)^2 - 1\right] \tag{4.3.5}$$

$$\beta_{1SD} = \beta_{10} \gamma \rho(1-\rho^2)$$

in which

$$\gamma = \frac{12D(1+\nu)}{GHb^2} \tag{4.3.6}$$

which for (4.0.3) is

$$\gamma = 6(1+\nu) (E/G) (hH/b^2) \tag{4.3.7}$$

For a thin panel, both the face thickness and the honeycomb thickness H are small in comparison with the radius b, so that γ will tend to be small and (4.3.5) will be negligible in comparison with the instantaneous elastic response (4.1.5, 4.1.7). For honeycomb, however, the effective shear modulus G is small in comparison with E for the faces, so that γ (4.3.7) can be of the order of unity or larger.

For a material which, when loaded at time t = 0, reaches a stable displacement at time t = τ, a simple Kelvin (or Voight) viscoelastic model can be used. This model consists of a spring and dashpot in parallel, and has the longtime elastic constant (G) and the time τ for parameters. The correction to (4.3.5) is just

$$w_{1SD} = \beta_{10}\gamma(b/4)\,[(1-\rho^2)^2-1](1-e^{-t/\tau})$$

$$\beta_{1SD} = \beta_{10}\gamma\,\rho(1-\rho^2)\,(1-e^{-t/\tau}) \qquad (4.3.8)$$

To summarize, the complete springback consists of the instantaneous reponse of the purely elastic face plates (4.1.1 - 4.1.7) followed by a viscous flow of the honeycomb core and adhesive (4.3.8) which stabilizes in time τ. This behavior is shown in Fig. 4.4.

5.0 HOT SPOT STRESS

The thermal stresses due to heating of the glass face plate in a circular spot can be calculated from a plane stress analysis, i.e. from (2.1.2) with the change in guassian curvature F set equal to zero

$$\Delta\Delta\Phi = 0 \tag{5.1}$$

when the condition (4.0.6) is satisfied. The essential features can be obtained from an axisymmetric analysis. We consider a region $0 \leq r \leq a$ uniformly heated to the temperature T_0 in a plate of outer radius b. The solutions for the heated and unheated regions are

$$\left.\begin{aligned} \sigma_r &= \sigma_\theta = -A \\ E\varepsilon_\theta &= \sigma_\theta - \nu\sigma_r = -A(1-\nu) + E\alpha T_0 \end{aligned}\right\} \quad 0 \leq r \leq a$$

$$\left.\begin{aligned} \sigma_r &= B(1-b^2/r^2) \\ \sigma_\theta &= B(1+b^2/r^2) \\ E\varepsilon_\theta &= B(1-\nu+(1+\nu)b^2/r^2) \end{aligned}\right\} \quad a \leq r \leq b \tag{5.2}$$

At r=a the displacement and stress must be continuous which gives the constants

$$A = B(-1+b^2/a^2) \tag{5.3}$$

$$B = E\alpha T_0 a^2/2b^2$$

The circumferential tensile stress in the outer (cold) region has its maximum value at r = a

$$\sigma_\theta = \frac{E\alpha T_0}{2}\left(1 + \frac{a^2}{b^2}\right) \tag{5.4}$$

The stress distribution for the infinite plate $b \to \infty$ is shown in Fig. 5.1.

Since the stress in the cold region decays rapidly, this thermal stress is localized and can be used for other than the circular panel. If the spot is far from the boundaries of the rectangular panel, then

$$\sigma_\theta \cong E\alpha T_o/2 \tag{5.5}$$

However, if the spot is near the edge of the rectangular panel, then the most severe situation occurs

$$\sigma_\theta \cong E\alpha T_o \tag{5.6}$$

An analysis of the complete panel with the hot spot on one face leads to the same result (5.4). Only when the back plate has a substantially higher bending stiffness than the glass sheet will the thermal stress be decreased from (5.4).

For a general temperature distribution in a plate, the equation is

$$\Delta\Delta\Phi = Eh\alpha\Delta T \tag{5.7}$$

For the more realistic (Agarwal, 1980) axisymmetric distribution

$$T = T_o \exp(-r^2/a^2) \tag{5.8}$$

the solution for the infinite plate ($b \to \infty$) is

$$\sigma_r = (E\alpha T_o/2)\,(-1+\exp(-r^2/a^2))a^2/r^2 \tag{5.9}$$

$$\sigma_\theta = (E\alpha T_o/2)\left[(1-\exp(-r^2/a^2))a^2/r^2 - 2\exp(-a^2/r^2)\right] \tag{5.10}$$

This distribution is shown in Fig. 5.2. For a finite disc with a free edge at r=b, a constant tension stress field must be added to Eqs. (5.9) and (5.10). The maximum circumferential tension for this case is shown by the dashed line in Fig. 5.2. Thus, the worst case is

$$\sigma_\theta = 0.30\ E\alpha T_o \tag{5.11}$$

which occurs when b = 1.3a. For the large plate $b/a \to \infty$, the maximum tension is

$$\sigma_\theta = 0.109\ E\alpha T_o \qquad (5.12)$$

Thus the smooth gradient in the temperature field does reduce substantially the maximum tensile stress. But still the worst situation occurs when the hot region is near a free edge.

6.0 SURVEY OF GLASS FRACTURE STRENGTH
(by D. Nelson)

6.1 - Short-Time Fracture Strength

Typically, mechanical engineering design handbooks only provide values of glass fracture strength determined from tests of very short duration (seconds or less). For example, Kent's Mechanical Engineer's Handbook (1967) specifies a range of 4 to 10 ksi for typical annealed soda-lime glass. It specifies the same range for a variety of other glasses, including lead, borosilicate and 96% silica glasses and fused quartz. It also notes that "for safe design practice, tensile stresses should be limited to 1000 psi for annealed glass," but does not elaborate on the rationale for this statement.

Values of facture strength for specimens with a semi-circular flaw of .002 in. depth are given by Shand (1961) and are shown in Table 1. In this case, the test duration was one second.

Table 1 - Short-Time Fracture Strength of Glass

Type of Glass	Strength (ksi)
lead alkali	6.8
soda-lime	9.0
96% silica	11-12
borosilicate (low expansion)	12
aluminosilicate	13.8

Such short-time strength values are deceptively high for components which must sustain tensile stress over any significant period of time.

6.2 - Stress Corrosion Cracking ("Static Fatigue")

It has been well-established that the bulk strength of glass is governed by the presence and fracture behavior of small flaws, particularly at the surface. When glass experiences sustained tensile stress, it suffers a time-dependent loss of strength, as illustrated

in Fig. 6.1. This phenomenon, originally termed "static fatigue,"is now known to be due to the growth of small initial flaws to a critical size by a stress corrosion cracking mechanism. This mechanism is activated by adsorption on flaw surfaces of water vapor or other corrosive media. The rate of crack growth and thus the fracture strength - time behavior is strongly dependent on glass composition, relative humidity and temperature, as will be discussed later.

The fracture strength-time behavior of specimens of soda-lime window glass, with artificially-induced .002 in. deep semi-circular flaws is discussed by Shand (1961) and is shown in Fig. 6.2. Tests were conducted at room temperature and in uncontrolled humidity. For tests lasting 10^6 secs. (about one month), the fracture strength was approximately 4 ksi in reannealed specimens. It is not clear from the data whether or not a "static fatigue limit" exists. The as-received specimens displayed a greater resistance to stress corrosion cracking, perhaps due to surface compressive residual stresses, which were relieved in the re-annealed specimens. Fig. 6.3 provides a comparison of soda-lime fracture strength-time behavior with that of low expansion borosilicate, for the same test conditions.

The stress corrosion behavior of soda-lime specimens, as discussed by Mould and Southwick (1959), tested in distilled water and containing various surface abrasions is shown in Fig. 6.4. These data clearly demonstrate the important influence of both initial defect depth and defect orientation with respect to applied tensile stress. Again, it is not clear from these data whether or not a "safe" stress exists for long-time service. At 10^3 secs., the strength is already reduced to about 4 ksi for scratches (line defects) of .0009 in. depth. At this point, it should be noted and emphasized that all of the data considered represent only median (50% failure probability) behavior.

Stress corrosion data have also been published in terms of fracture strength vs. stress or loading rate. For example, Ritter (1973) shows that a relation of the following form provides a good

correlation between strength and stress rate:

$$\sigma_f = KB^{\frac{1}{m+1}} \tag{6.1}$$

where:

σ_f = fracture strength

$B = \frac{\text{stress-rate (psi/min)}}{3 \times 10^5}$

K,m = empirical constants for a given environment and glass type.

For abraded soda-lime glass, K ≃ 11.7 ksi and m = 13-16. If, for example, the applied stress is 5 ksi, acting over a 10 year period, then $B = 3 \times 10^{-9}$ psi/min. In this case, predicted σ_f would range between 2.5 and 3.5 ksi (depending on m), if extrapolation to such long lives is valid.

6.3 - Fracture Mechanics Evaluation of Stress Corrosion Cracking

The previous data were generated before the widespread use of linear elastic fracture mechanics to interpret crack propagation behavior. During the past decade, stress corrosion cracking has been correlated in terms of the mode I stress intensity factor, K_I. The rate of growth, da/dt, is often found, as shown by Evans and Johnson (1975), to follow the form given in Fig. 6.5, for constant stress tests. The behavior in region I, where most of the life is spent, is described by:

$$da/dt = AK_I^n \tag{6.2}$$

$$K_I = f(G)\sigma(\pi a)^{\frac{1}{2}} \tag{6.3}$$

where:

f(G) = function of crack/geometry type and loading type

σ = applied nominal stress

a = crack depth

A,n = empirical constants depending on environment and glass type

Growth rate is very sensitive to relative humidity, as shown by Wiederhorn (1974). For instance, the region I rate of soda-lime-silica glass at 0.2% R.H. is about ten times greater than at a reference rate of 0.017% R.H., for the same K_I. At 10% R.H., the rate is approximately a hundred times larger than the reference rate. Growth rate can also be quite sensitive to temperature. Tests of soda-lime glass in vacuum showed the rate at 214°C to be roughly a thousand times higher than at room temperature, as given by Wiederhorn, et al. (1974a). In tests conducted in water, the growth rate of soda-lime-silica glass at 90°C was approximately a hundred times greater than at room temperature, as discussed by Wiederhorn and Bolz (1970).

The fracture toughness of most glasses falls between 0.75 and 1.0 ksi $(in)^{\frac{1}{2}}$, as shown by Wiederhorn (1969). Threshold stress intensity appears to be about 0.25 ksi $(in)^{\frac{1}{2}}$ for soda-lime glass at 25°C and about 0.2 ksi $(in)^{\frac{1}{2}}$ at 90°C, as discussed in Cekirge, et al. (1976). (There is some uncertainty, though, as to whether a threshold really exists.)

The significance of threshold stress intensity is that if initial defect size(s) is known, then stress levels can be computed which will presumably prevent growth over the service life of a glass component. For example, suppose that initial surface defects are semi-circular, of depth a. The applied K_I, as shown in Tada, et at. (1973), will be:

$$K_I \cong 0.92\ \sigma\ (\pi a)^{\frac{1}{2}} \qquad (6.4)$$

(This expression is for uniform tensile stressing, but is also an excellent approximation for bending stress in the case of small surface flaws.) Using a value of K_{th} of 0.2 ksi $(in)^{\frac{1}{2}}$, and solving Eq. 6.4 for σ in terms of various a values gives the results shown in Table 2.

Table 2 - Estimated Threshold Stress for Semi-Circular Surface Flaws

Crack Depth (in.)	Threshold Stress (ksi)
.0002	8
.0005	5.5
.001	3.9
.002	2.7

Similar calculations were done for line defects (scratches), using

$$K_I \cong 1.12\ \sigma\ (\pi a)^{\frac{1}{2}} \tag{6.5}$$

Results are given in Table 3.

Table 3 - Estimated Threshold Stress for Uniform Depth Edge Flaws

Crack Depth (in.)	Threshold Stress (ksi)
.0002	7
.0005	4.5
.001	3.2
.002	2.2

The values in Table 3 appear to be in reasonable agreement with projections of the curves in Fig. 6.4 for corresponding flaw depths.

It is worth noting that even if K_{th} does not exist, crack growth rate data of the type mentioned previously could be used to estimate or bound service life by combining Eqs.6.2 and 6.3 and integrating, i.e.,

$$t_{life} = \frac{1}{Af^n(G)\sigma^n} \int_{a_{initial}}^{a_{critical}} (\pi a)^{-n/2} da \qquad (6.6)$$

(Such analysis was beyond the scope of this effort.)

The data considered thus far have been for steady stress. According to Tetelman and McEvily (1967), stress corrosion long-life strength under cyclic or steady stress is essentially the same, based on the very limited cyclic data available. Crack growth under cyclic stress in glass appears to be due to the same type of mechanism which causes growth under static loading. Wachtman (1974) gives a fracture mechanics-based method for evaluating growth rate under a steady stress and superposed cyclic stress, utilizing only test data from static tests. In any case, it should be conservative for design purposes to use maximum stress or stress intensity (sum of static and amplitude of alternating component) to assess fracture strength-time behavior or rate of growth, respectively.

Little if any data on the stress corrosion behavior of glass experiencing cyclic thermal stress appear to exist. Virtually all studies on the fracture resistance of glass to thermal stress have been concerned with behavior under quenching.

6.4 - Summary of Fracture Strength Data

For long lives (years) in the presence of any humidity (even a few %), it appears that median fracture strength is on the order of 2-3 ksi, at least for representative soda-lime glass. This is based on conventional σ_f - t and on K_{th} data. The strength will depend largely on actual initial defect sizes. There are not sufficient data to establish with confidence allowable stresses for very low probabilities

of failure. However, limited data from Evans and Johnson (1975) suggest that fracture strength for 10% probability of failure is about 60% of that for a median probability.

6.5 - Methods to Improve Fracture Strength

Long-life fracture strength can be significantly increased by protective coatings or by producing surface compressive residual stresses. Polymeric coatings such as epoxy or acrylic resins can increase strength by at least 50%, as discussed by Ritter (1973), by inhibiting moisture adsorption. Surface compressive residual stresses of 10-15 ksi can be produced, as shown in Tetelman and McEvily (1967), by chill tempering and will help reduce corrosion crack growth.

6.6 - Proof Testing

The lifetime of glass components will be governed primarily by the behavior of the few largest initial flaws. In order to avoid premature failure, proof-testing has been suggested by Wiederhorn, et al. (1974b) in order to detect those components with unacceptably large defects. If a proof stress σ_p, is applied, producing a corresponding K_{IP}, then surving components must have $K_{IP} = f(G)\sigma_p(\pi a_0)^{\frac{1}{2}} < K_{IC}$ thus "assuring" no defects larger than a_0. Initial crack size, a_0, can then be used with a fracture mechanics-based analysis of stress corrosion crack growth rate to estimate a minimum expected life.

7.0 CROSBYTON PANELS

The panels developed for the CROSBYTON SOLAR POWER PROJECT have the following properties (Perry, 1980)

$$\begin{aligned} h &= 3/32 \text{ in} \\ L = L_y &= 19.5 \text{ in} \\ R &= 37.5 \times 12 \text{ in} \\ H &= 2 \text{ in} \\ h_s &= 0.024 \text{ in} \\ E_s &= 30 \times 10^6 \text{ psi} \end{aligned} \tag{7.1}$$

For the glass plate we take the values

$$\begin{aligned} E &= 10.4 \times 10^6 \text{ psi} \\ \nu &= 0.3 \\ \alpha &= 9 \times 10^{-6}/^{o}C \end{aligned} \tag{7.2}$$

and the temperature above ambient of the hot spot measured by Agarwal (1980) is

$$T_o = 122^{o}C \tag{7.3}$$

7.1 - Calculations of Stress and Springback

The important stress factors are

(1) Residual stress in bending (2.1.9)

$$\sigma_{BO} = \frac{Eh}{2(1-\nu)R} = \frac{(10.4\times10^6)(3/32)}{2(0.7)(37.5 \times 12)} = 1{,}550 \text{ psi} \tag{7.4}$$

(2) Residual membrane stress
Nominal value (3.2.3)

$$\sigma_{DO} = \frac{EL^2}{8R^2} = \frac{(10.4\times10^6)(19.5)^2}{8(37.5 \times 12)^2} = 2{,}440 \text{ psi} \tag{7.5}$$

Tension at center of square plate (Fig. 3.5)

$$(\sigma_D)_{Max} = 0.56\ \sigma_{DO} = 1{,}370 \text{ psi} \tag{7.6}$$

Compression at center of edge

$$(\sigma_D)_{Min} = -\ 1.6\ \sigma_{DO} = -\ 3{,}900 \text{ psi} \tag{7.7}$$

(3) Thermal tensile stress due to hot spot.
For spot away from edges (5.11)

$$\sigma_T = 0.109\ E\alpha T_o = 0.109(10.4\times10^6)(9\times10^{-6})(122)$$
$$= 1{,}250 \text{ psi} \tag{7.8}$$

For spot near edge (5.12)

$$\sigma_T \cong 0.30\ E\alpha T_o = 3{,}430 \text{ psi} \tag{7.9}$$

The residual tension is maximum at the panel center in the surface of the glass bonded to the honeycomb, which is the sum of the membrane (7.6) and bending (7.4) stresses

$$(\sigma)_{\substack{\text{Residual} \\ \text{at center}}} = \sigma_{BO} + 0.56\ \sigma_{DO} = 2{,}920 \text{ psi} \tag{7.10}$$

The short-time thermal stress (7.8) is added to this to give the peak stress

$$(\sigma)_{\substack{\text{Peak at} \\ \text{center}}} = 2{,}920 + 1{,}250 = 4{,}170 \text{ psi} \tag{7.11}$$

Near the center of the edge, the maximum residual stress is slightly compessive, the sum of (7.4) and (7.7)

$$(\sigma)_{\substack{\text{Residual} \\ \text{at edge}}} = 1{,}550 - 3{,}900 = -2{,}350 \text{ psi} \tag{7.12}$$

which alleviates somewhat the high thermal stress (7.9)

$$(\sigma)_{\substack{\text{Peak at}\\ \text{edge center}}} \cong -2{,}350 + 3{,}430 = 1{,}080 \text{ psi} \tag{7.13}$$

However, near the corner the membrane compression is small while (7.4) and (7.9) remain active

$$(\sigma)_{\substack{\text{Peak near}\\ \text{corner}}} \cong 1{,}550 + 3{,}430 = 4{,}980 \text{ psi} \tag{7.14}$$

The reference springback rotation is (4.1.6)

$$\begin{aligned} \beta_{10} &= 0.00729\ b^5/H^2R^3 \\ &= 0.00729\ (19.5)^5/(2)^2(37.5\text{x}12)^3 \\ &= 56 \times 10^{-6} \text{ rad} \\ &= 0.0032 \text{ degrees} \end{aligned} \tag{7.15}$$

so the displacement at the corner of the square panel (Fig. 4.1) is

$$\begin{aligned} (w_1)_c &= 1.02\ \beta_{10}\ L \\ &= 1.02\ (56 \times 10^{-6})(19.5) \\ &= 0.0011 \text{ in} \end{aligned} \tag{7.16}$$

The additional springback at the corner due to the bending stress (4.0.11) is

$$\begin{aligned} (w_{B1})_c &= L^2h^2/RH^2G(1-\nu^2) \\ &= (19.5)^2(3/32)^2/(37.5\text{x}12)(2)^2 6(.91) \\ &= 0.00034 \text{ in} \end{aligned} \tag{7.17}$$

which gives the total corner springback displacement

$$(w_1)_c = 0.0011 + 0.00034$$
$$= 0.0014 \text{ in} \qquad (7.18)$$

Note that this is the instantaneous elastic springback and does not include any viscous softening of the core. The springback rotation at the corner is (4.2.4)

$$(\beta_1)_c = 2.44\ \beta_{10}$$
$$= 2.44\ (0.0032^o) = 0.0078^o \qquad (7.19)$$

and the additional rotation due to the bending stress (4.0.11) is

$$(\beta_{B1})_c = (w_{B1})_c\ 2^{\frac{1}{2}}/L$$
$$= (0.00034\text{in})\ 2^{\frac{1}{2}}/(19.5\text{in})$$
$$= 0.0014^o \qquad (7.20)$$

so the total is

$$(\beta_1)_c = 0.0078 + .0014 = 0.0091^o \qquad (7.21)$$

The maximum tension in the adhesive due to the membrane stress in the glass plate occurs at the center of the panel. For the circular panel (3.2.5) this is

$$(\sigma)_{\substack{\text{Adhesive} \\ \text{panel center}}} = Ehb^2/8R^3$$

and for the square panel (Fig. 3.9)

$$(\sigma)_{\substack{\text{Adhesive}\\ \text{panel center}}} = 1.13\ EhL^2/8R^3$$

$$= 1.13\ (10.4\text{x}10^6)(3/32)(19.5)^2/8(37.5\text{x}12)^2$$

$$= 0.58 \text{ psi} \qquad (7.22)$$

However, in the edge region, perfect conformity of the glass to the spherical curvature requires the stress in the adhesive (3.4.12)

$$(\sigma)_{\substack{\text{Adhesive}\\ \text{near edge}}} = 0.14\ \sigma_{BO}$$

$$= 0.14\ (1550) = 217 \text{ psi} \qquad (7.23)$$

This is a high demand for an adhesive. Unlike the stress (7.22) which is over a substantial area in the panel center, (7.23) occurs on a highly localized strip about one plate thickness from the edge and with a width of about one plate thickness, as shown in Fig. 3.11. The compressive stress in the honeycomb at the edge is

$$(\sigma)_{\substack{\text{Compression}\\ \text{at edge}}} = 0.94\ \sigma_{BO}$$

$$= 1460 \text{ psi} \qquad (7.24)$$

7.2 - Comparison with Tests and Field Experience

The levels of residual and peak stresses (7.4) - (7.14) when compared to the behavior of glass indicated by Figs. 6.1 - 6.4 do not give much encouragement to the prospects for long-term life of the Crosbyton panels. Since these curves give median (50% failure) the experience to date discussed by Perry (1980) seems to fit. The residual tension at the panel center (7.10) is high enough to cause cracking in a few panels, presumably those with large flaws, during fabrication. The subsequent experience with the prototype system reported by W.H. McCulloch (pers. comm.) is that some 20% of the panels have cracked due to the hot spot. The peak stresses at the corner (7.14), edge (7.13) and at the center (7.11) sustained for a few minutes would

certainly cause cracking, if the curve in Fig. 6.4 for 600 grit cloth is similar to the glass used by E-Systems.

The springback was a major concern in developing the fabrication procedure, however, little quantitative information is given by Perry (1980). One panel was permitted to cure extra time and apparently had little viscous flow for 50 hours and had a maximum springback displacement of 0.002 in. (Perry, 1980), p.21) D.B. Longcope (pers. comm.) reports that generally a deflection of the corner of about 0.004 in. occurs in about four days. This is larger than the calculated value for the instantaneous elastic response (7.18) and indicates the viscoelastic behavior of the core shown in Fig. 4.4.

The deviation of the angle of the normal to the surface which is calculated (7.21) is substantially less than shown by the laser scan of Panel No. 20 (Fig. 4.5) which has maximum values of 0.20 degrees. Most of this deviation must be attributable to imperfection of the mold rather than springback.

The level of tensile stress in the adhesive in the center of the panel (7.17) should be no problem. That required in the strip near the edge (7.18) is cause for concern and may be the source of edge debonding. The compressive stress in the honeycomb at the edge (7.19) is very high. From information from D.B. Longcope (pers. comm.) a sample of the honeycomb was subjected to a compression test on May 1, 1979, and failed at a stress of 545 psi. We conclude that local crushing of the honeycomb probably occurs which decreases the magnitude of stress from that shown in Fig. 3.11, and which has the negative effect of leaving the edge region with a substantial deviation from the spherical curvature. The width of this deviation should be no more than three plate thicknesses which would not cause a substantial loss in panel efficiency.

8.0 RECOMMENDATIONS

8.1 - Tests to Validate Analysis

We have a reasonable confidence in the analysis presented in the preceding Sections of this Report. The basic equations are well-established, and the simple closed-form results for the circular plate and the plate strip give limits on the numerical results for the square and low aspect ratio plates, which indicates that no serious errors in the solutions are present. The more serious question concerns the validity of the mathematical models. The residual stress in the initially flat, thin glass plate deformed to a shallow spherical surface should be very accurately described by the equations used, so that comparison with experiment would serve more as a calibration of the experimental technique.

The springback analysis less precisely reflects the reality of the panels fabricated by E-Systems. Particularly the steel backplate has been assumed to be completely flexible during the forming process, but to have full strength in resisting the springback. The E-Systems technique of slotting the steel plate (Fig. 1.3) does decrease substantially its resistance to forming, and filling the slots with epoxy does restore substantially the resistance to springback, but certainly not uniformly. The final angular deviation measured in one panel (Fig. 4.4) is an order of magnitude larger than calculated and is unexpectedly irregular. On the other hand, the magnitude of springback deflection reported is consistent with the calculation. The tentative conclusion is that the deviation shown in Fig. 4.4 is largely due to mold imperfection. The importance of the final angular deviation to the efficiency of the panel requires a careful study to isolate the contributing factors, namely the mold imperfection, the instantaneous elastic springback as affected by the slotted backplate, and the viscous flow of the epoxy stiffening the honeycomb core. For this, more detailed measurements such as in Fig. 4.4 and detailed surface displacement measurements should be made at various times after release of the panel from the

mold. If these factors are known and under tight control, then the modification of the mold surface such that springback would be to the desired exact spherical shape could be easily calculated.

The most severe difficulty to the present system is the hot spot thermal stress. The temperature difference measured by Agarwal (1980) gives high stresses which would cause cracking of the glass. This stress (7.8, 7.9) is independent of glass thickness, panel thickness, size of the spot, etc., so very little can be done in the way of design modifications to alleviate this stress. We note that the realistic smooth temperature profile does cause a lower stress than a uniformly hot "spot".

8.2 - Limitations and Requirements for Future Designs

The severe limitation seems to be the hot spot thermal stress which, as previously mentioned, is little affected by most of the design parameters of the panel. Stresses of the magnitude given by (7.11) and (7.14) sustained for 10 seconds will cause cracking of glass (Fig. 6.4). To avoid cracking, the quality of the glass must be improved and/or the defect size reduced, both of which increase cost.

Secondary to the short time, hot spot stress is the residual stress (7.10) which exceeds the generally recommended long-time stress level of 1000 psi, but is less than what seem to be long-time limiting values in Figs. 6.1, 6.2, 6.4. However, the extrapolation of these curves to 30 years (10^9 seconds) is probably not warranted, and the curves do represent only 50% of specimen. In short, the prospect of 30 year life for these panels is not good. These residual stresses do depend on the system dimensions. Doubling the radius of curvature, while keeping the panel size the same reduces the residual tension from 2,920 psi to 1,120 psi which would be satisfactory for 30 year life.

The instantaneous elastic springback (7.15), (7.16) does not seem to be a problem, and doubling R reduces this by a factor of 8.

The springback displacement varies with L^6, so doubling the panel size while holding the thickness of glass and honeycomb, and the radius R all fixed increases the springback by a factor of 64. This explains the difficulty experienced with the 6 ft x 4 ft panel (Perry, 1980) and the subsequent reduction to a 39in square panel.

The conclusion is that consideration of the design parameters on residual stress and springback, which have been obtained in this report, will permit reliable design of larger systems with larger panels using soda-lime float glass. The short time thermal stress due to the hot spot remains as a severe obstacle which requires further study. No economical means of avoiding cracking of the glass is evident at this time. There is the question of whether or not the efficiency of the panel is degraded by the cracking. A mechanical weakening of the panel against environmental loading and a leaking of moisture into the core certainly will result which will decrease the panel life.

REFERENCES

Agarwal, V.K. (1980), "The Thermal Behavior of Spherically Curved Solar Collector Mirror Panels Exposed to Concentrated Solar Radiation," M.S. Thesis, Texas Tech University.

Cekirge, H.M., Tyson, W.R. and Krausz, (1976), "Stress-Corrosion and Statique Fatique," J. Am. Ceram. Soc., Vol. 59, No. 5-6, pp. 265-266.

Evans, A.G. and Johnson, H., (1975), "The Fracture Stress and Its Dependence on Slow Crack Growth," J. Matls. Sci., Vol. 10, pp. 214-222.

Kent's Mechanical Engineer's Handbook,(1967),ed. C.Carmichael, J. Wiley & Sons, New York.

Mould, R.E. and Southwick, R.D., (1959), "Strength and Static Fatique of Abraded Glass Under Controlled Ambient Conditions: II, Effect of Various Abrasions and the Universal Fatique Curve," J. Am. Ceram. Soc., Vol. 42, No. 12, pp. 582-592.

Perry, J.L.(1980),"Mirror Panel Development, Testing and Production for Crosbyton Solar Power Project," Report ETC 80-001, E-Systems, Dallas, Texas.

Reissner, E. (1956), "A Note on Membrane and Bending Stresses in Spherical Shells," J. Soc. Indust. Appl. Math., 4, 230-240.

Ritter, J.E.,(1973),"Stress Corrosion Susceptibility of Polymeric-Coated Soda-Lime Glass," J. Am. Ceram. Soc., Vol. 56, No. 7, p. 402.

Shand, E.B. ,(1961),"Correlation of Strength of Glass with Fracture Flaws of Measured Size," J. Am. Ceram. Soc., Vol. 44, No. 21, pp. 451-455.

Steele, C.R. ,(1964),"Thermal Effects in Shells", Non-Classical Shell Problems, North Holland, 77-81.

Steele, C.R.,(1975),"Forming of thin shells," J. Appl. Mech, Vol. 42, p. 889.

Szilard, R.,(1974),Theory and Analysis of Plates, Prentice-Hall Inc.

Tada, H., Paris, P. and Irwin, G.,(1973),The Stress Analysis of Cracks Handbook, Del Research Corp., St. Louis.

Tetelman, A.S. and McEvily, A.J.,(1967),Fracture of Structural Materials, J. Wiley & Sons, New York, Fig. 12.7.

Von Kármán, T.,(1910), Enzyklopadie der Mathematischen Wissenschaften IV

Wachtman, J.B.,(1974),"Highlights of Progress in the Studies of Fracture of Ceramics and Glass," J. Am. Ceram. Soc., Vol. 57, No. 12, pp. 509-519.

Wiederhorn, S.M.,(1969),"Fracture Surface Energy of Glasses," J. Am. Ceram. Soc., Vol. 52, No. 2, pp. 95-105.

Wiederhorn, S.M. and Bolz, L.H.,(1970),"Stress Corrosion and Static Fatique," J. Am. Ceram Soc., Vol 53, No. 10, pp. 543-548.

Wiederhorn, S.M.,(1974),Fracture Mechanics of Ceramics, Vol. 2, Plenum Press, New York, pp. 613-646.

Wiederhorn, S.M., Johnson, H., Diness, A.M. and Hener, A.H.,(1974a), "Fracture of Glass in Vacuum," J. Am. Ceram. Soc., Vol. 57, No. 8, pp. 336-341.

Wiederhorn, S.M., Evans, A.G., Fuller, E.R. and Johnson, H.,(1974b), "Application of Fracture Mechanics to Space-Shuttle Windows," J. Am. Ceram. Soc., Vol. 57, No. 7, pp. 319-323.

APPENDIX

FIGURES

Fig. 1.1 - CROSBYTON SOLAR POWER PROJECT, Analog design verification system.

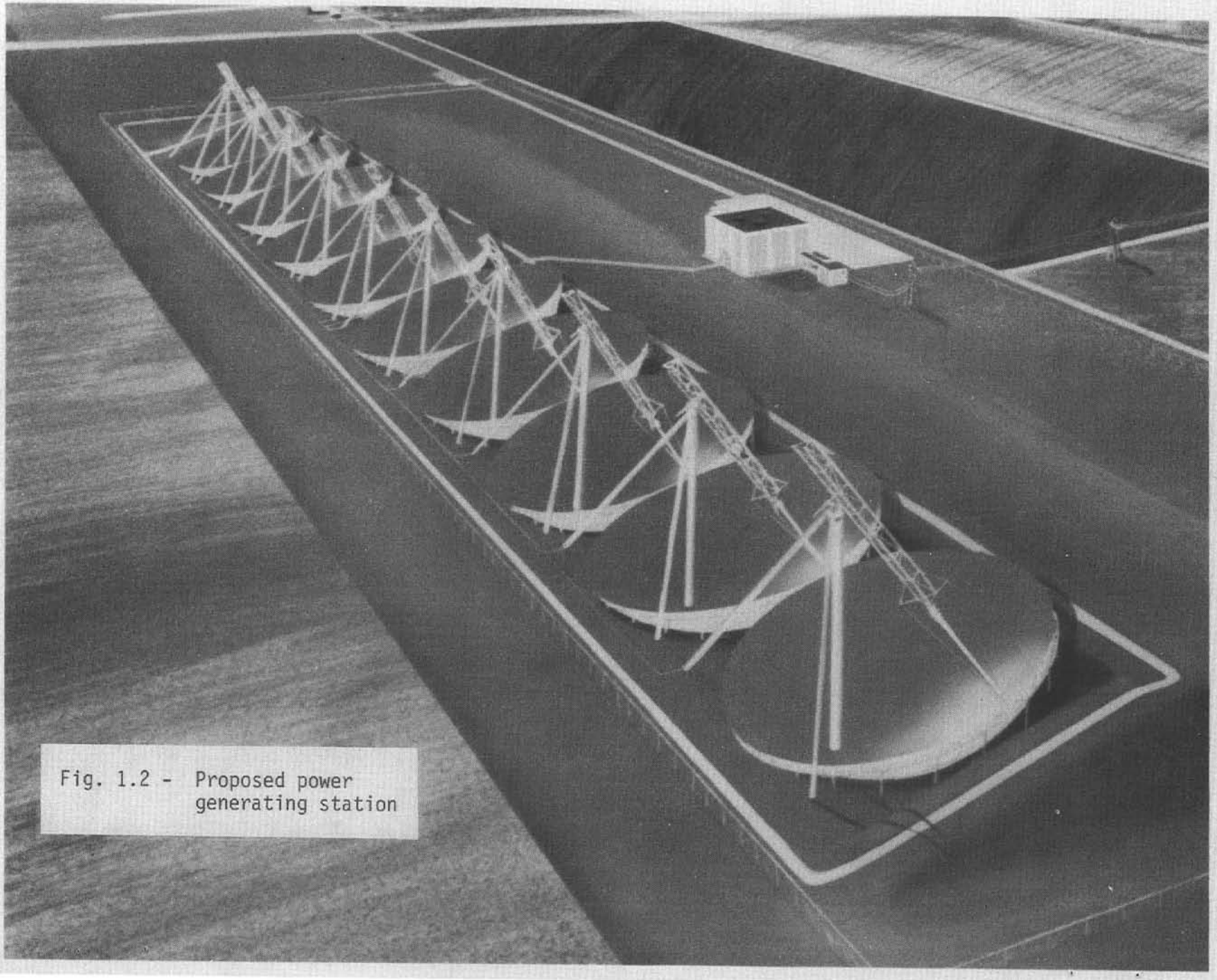

Fig. 1.2 - Proposed power generating station

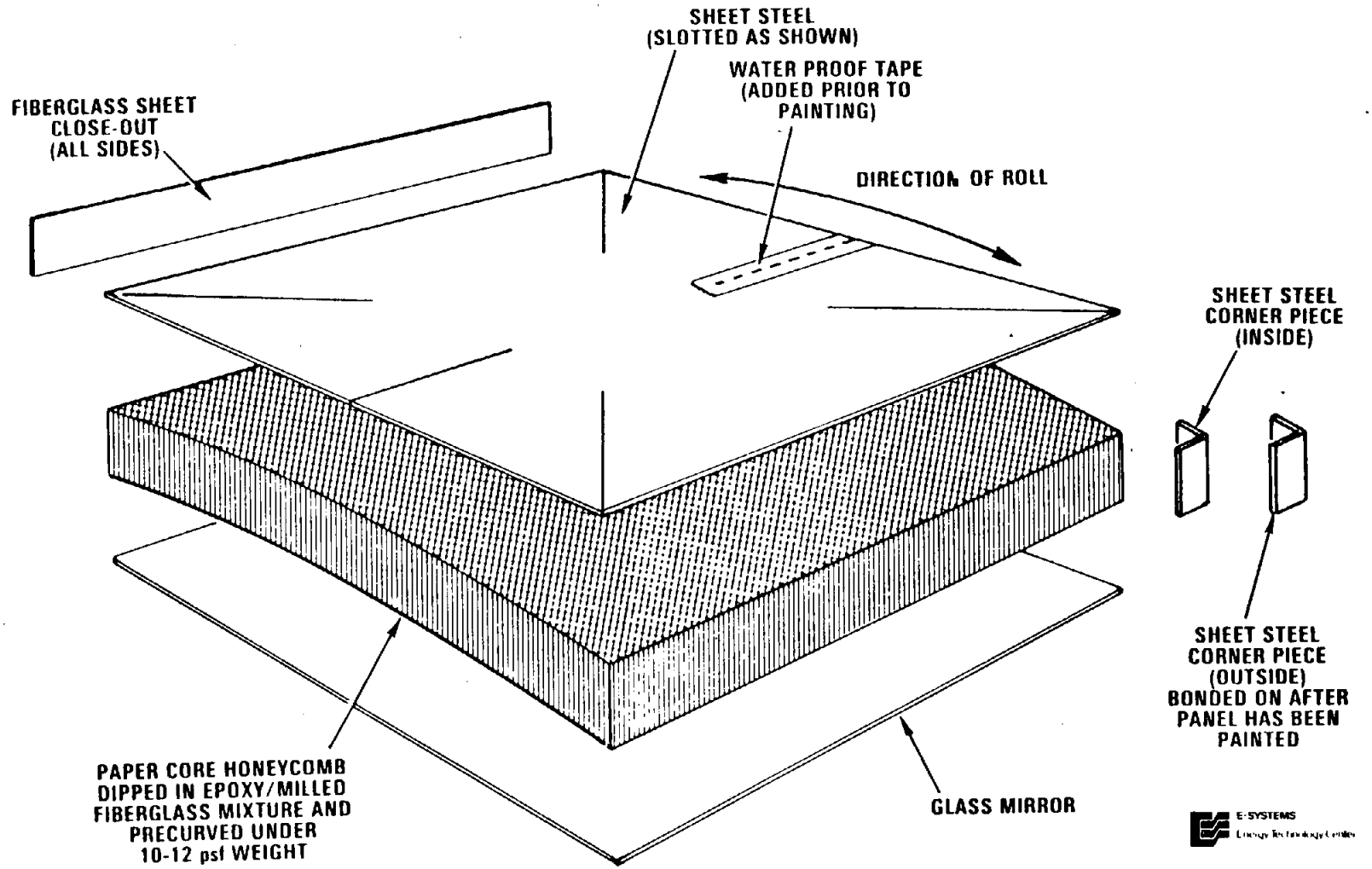

Fig. 1.3 - Mirror panel used in CROSBYTON SOLAR POWER PROJECT fabricated by E-Systems (from Perry, 1980)

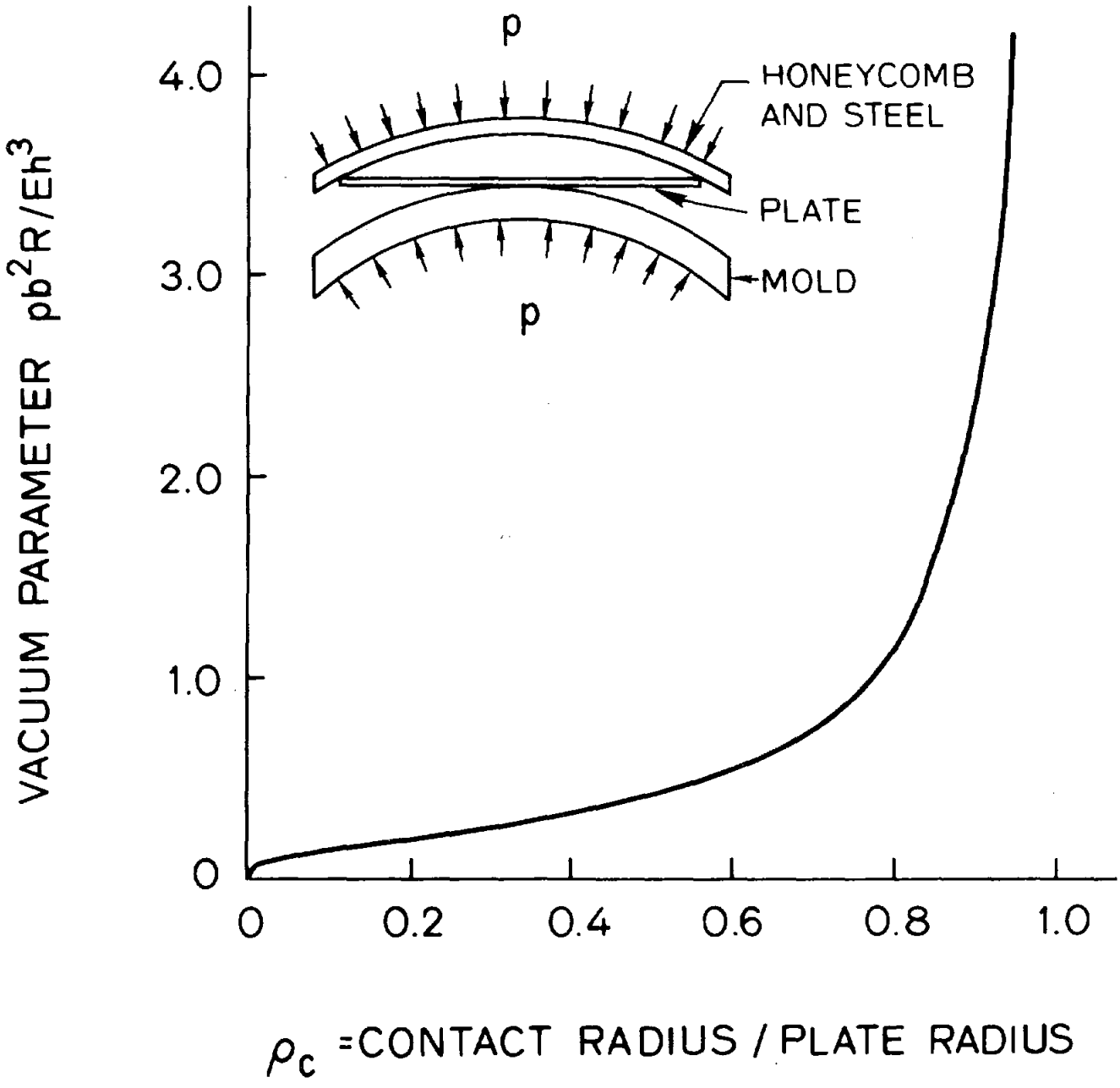

Fig. 2.1 - Relation of vacuum (p) to contact radius during deformation of circular plate (Young's modulus E, ν=0.3, radius b, thickness h) to rigid spherical surface (Radius of curvature R), neglecting membrane stresses.

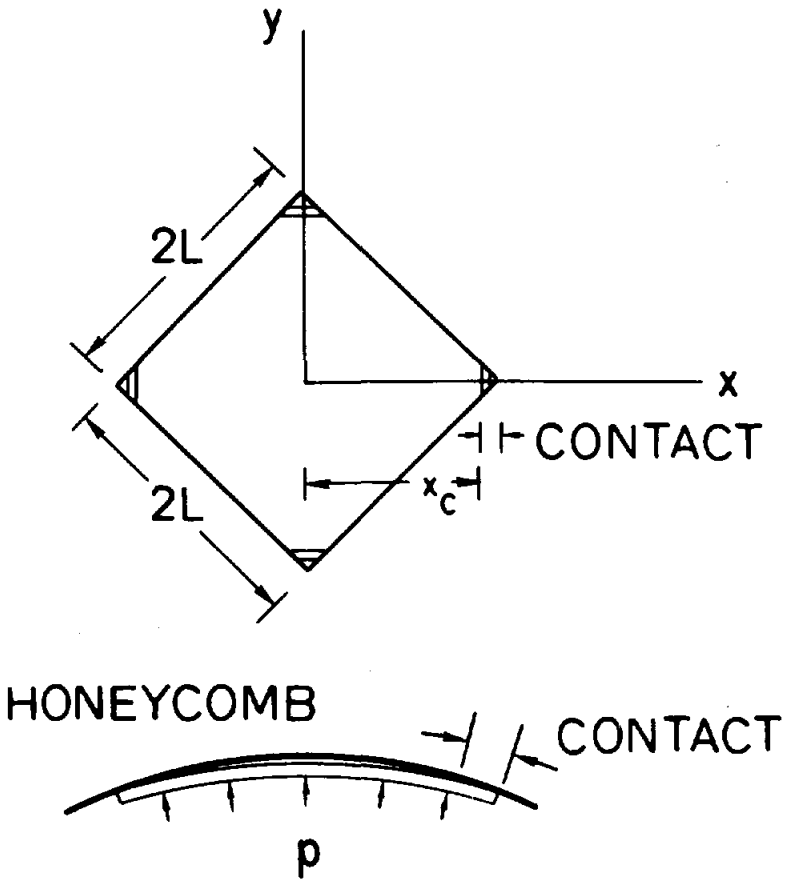

Fig. 2.2 - Initial loading of square plate in female mold (honeycomb). Large transverse shear stresses at corners occur.

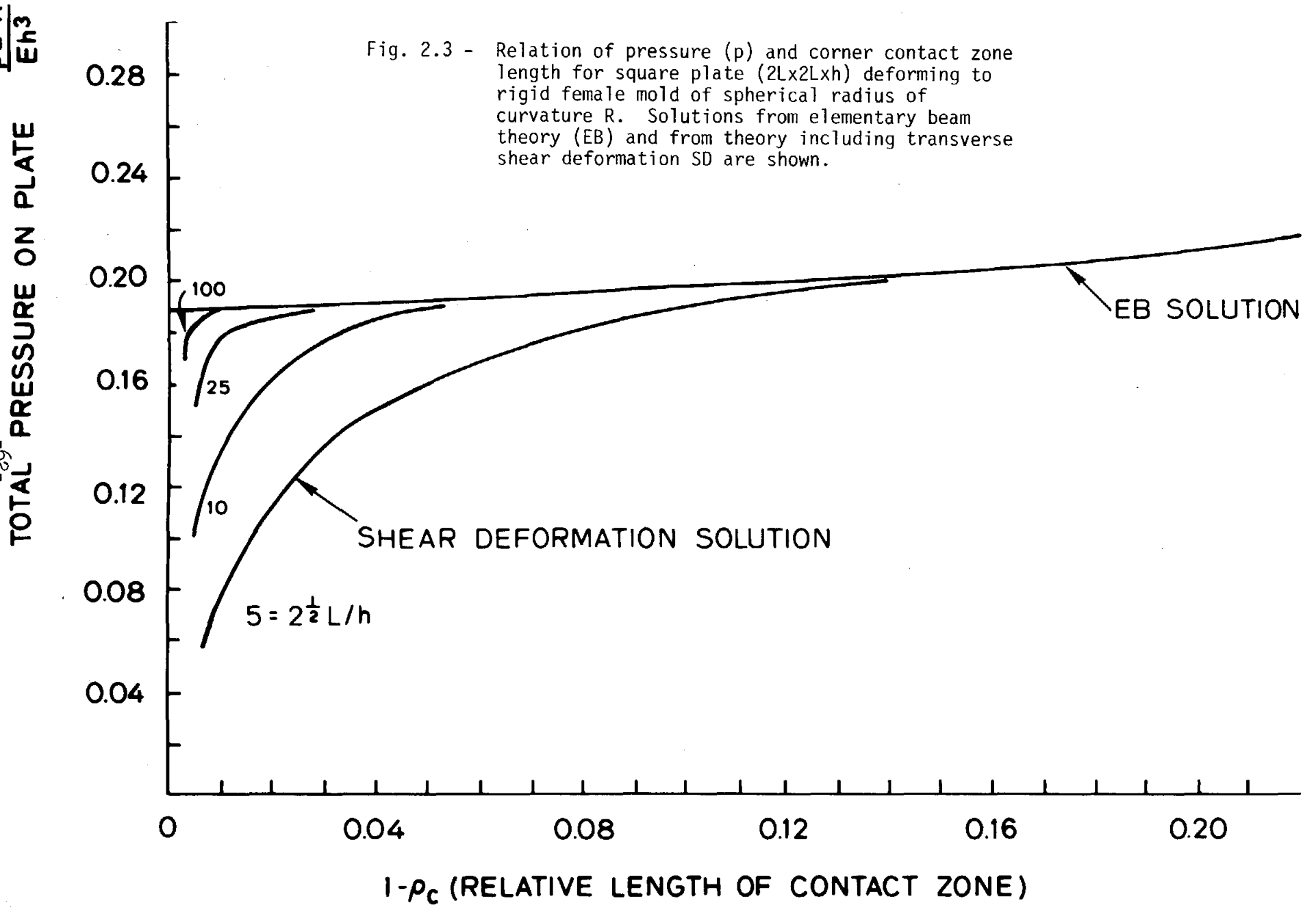

Fig. 2.3 - Relation of pressure (p) and corner contact zone length for square plate (2Lx2Lxh) deforming to rigid female mold of spherical radius of curvature R. Solutions from elementary beam theory (EB) and from theory including transverse shear deformation SD are shown.

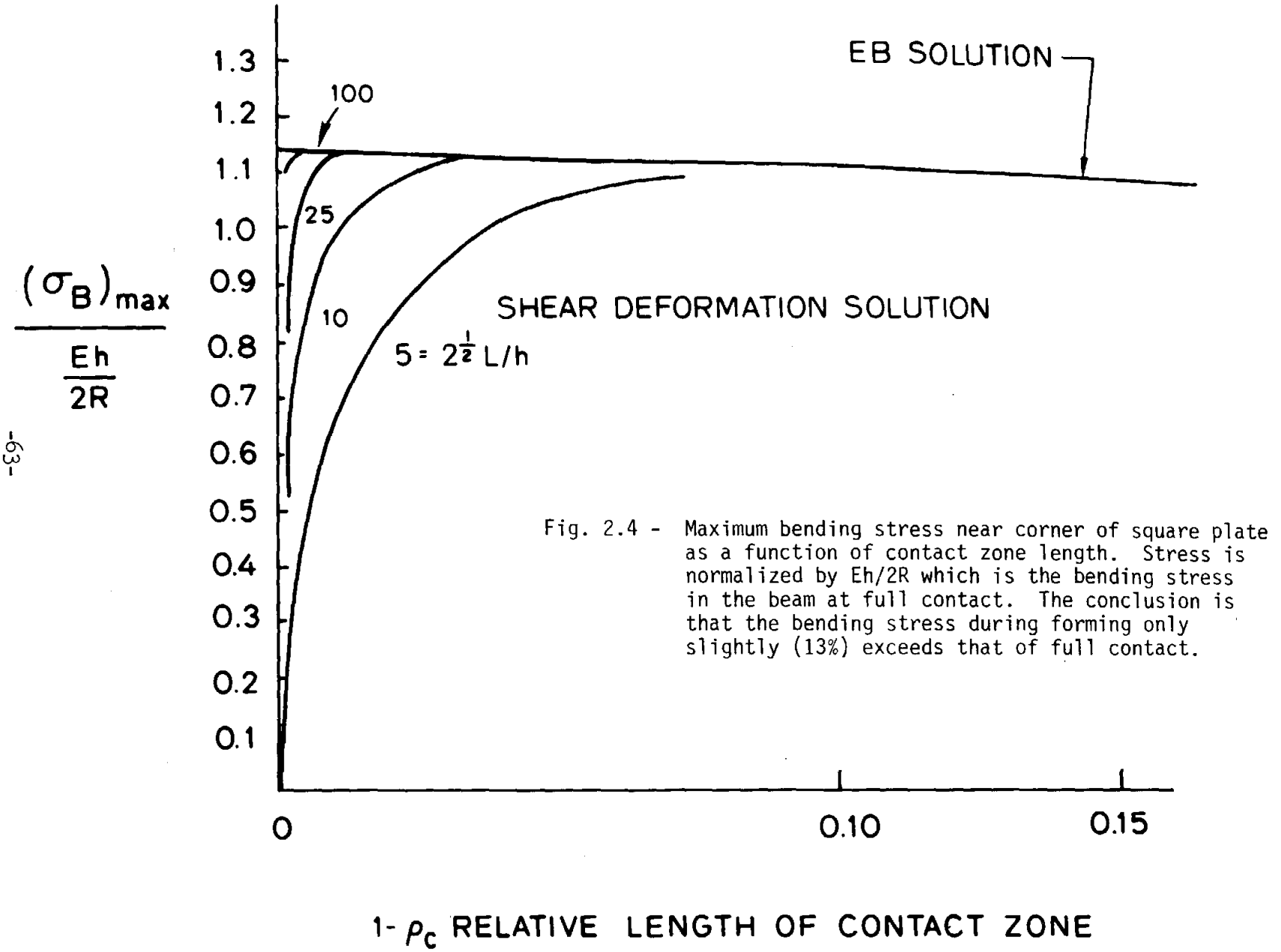

Fig. 2.4 - Maximum bending stress near corner of square plate as a function of contact zone length. Stress is normalized by Eh/2R which is the bending stress in the beam at full contact. The conclusion is that the bending stress during forming only slightly (13%) exceeds that of full contact.

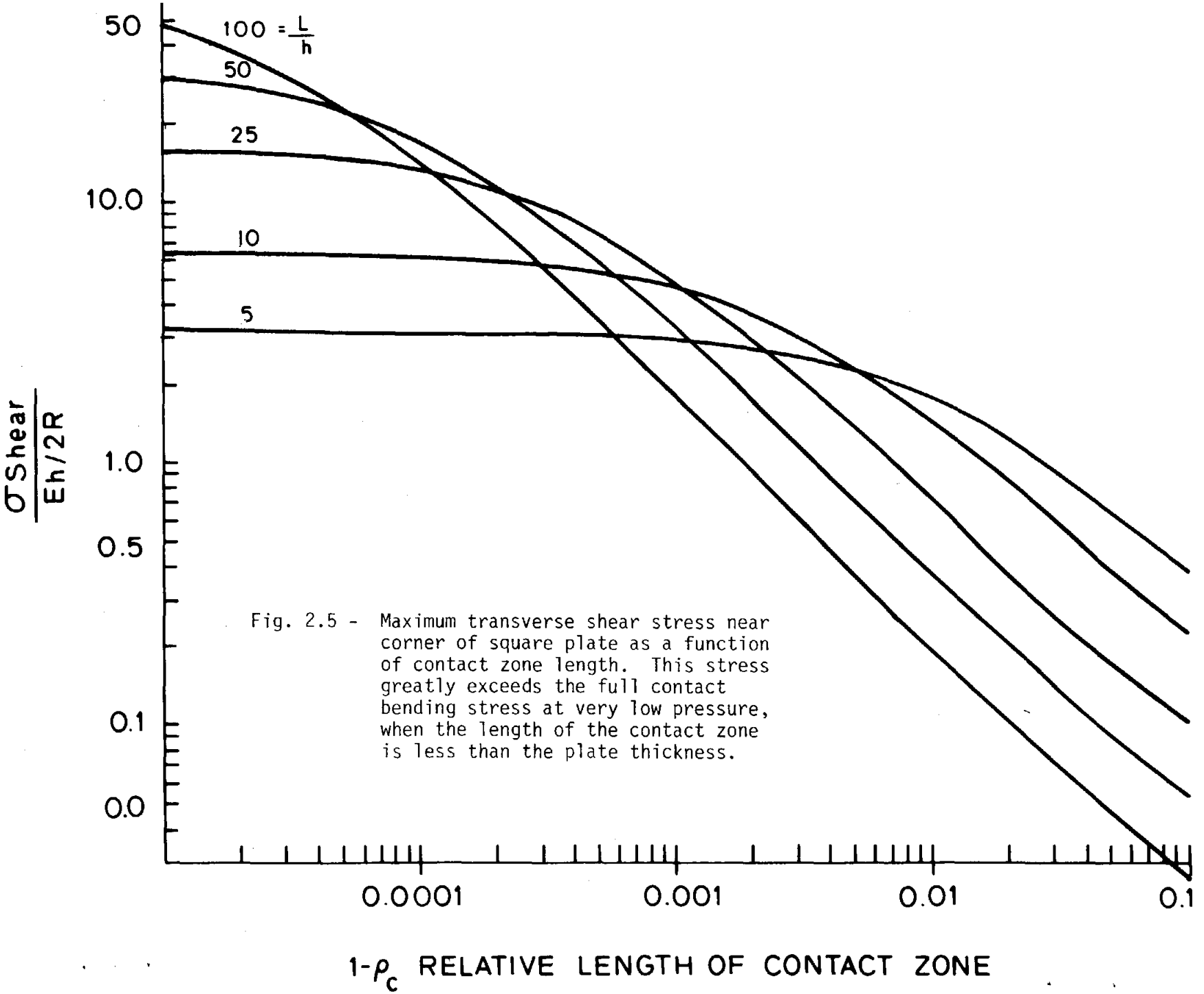

Fig. 2.5 - Maximum transverse shear stress near corner of square plate as a function of contact zone length. This stress greatly exceeds the full contact bending stress at very low pressure, when the length of the contact zone is less than the plate thickness.

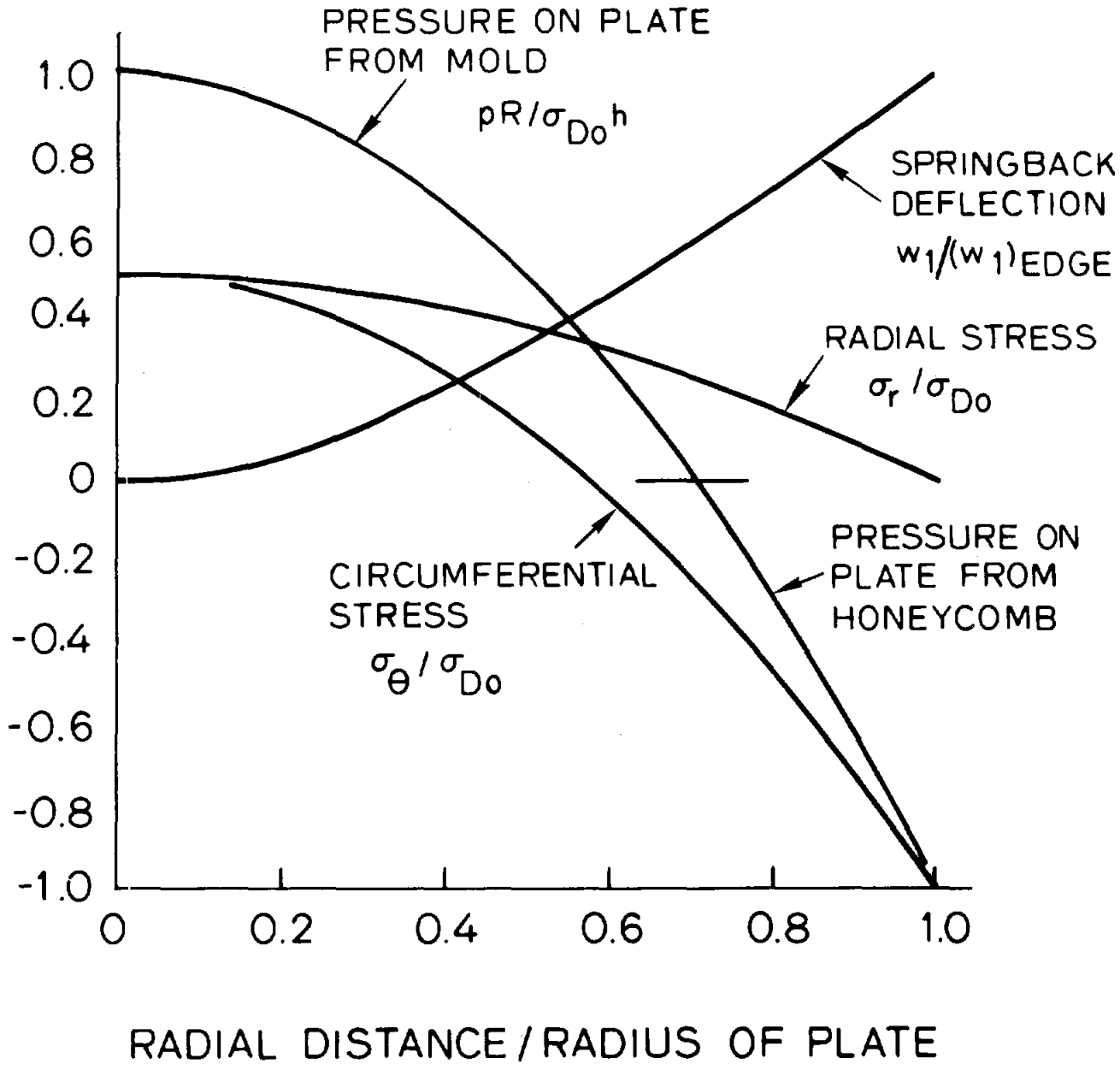

Fig 3.1 - Circular flat plate deformed to spherical surface. Maximum membrane stress is $\sigma_{DO}=Eb^2/8R^2$. After removal from mold, the springback at the edge is $(w_1)_{edge}= 0.00562\ b^6/H^2R^3$ where H is the thickness of the honeycomb. (Assumes steel backing has the same effective stiffness as the glass).

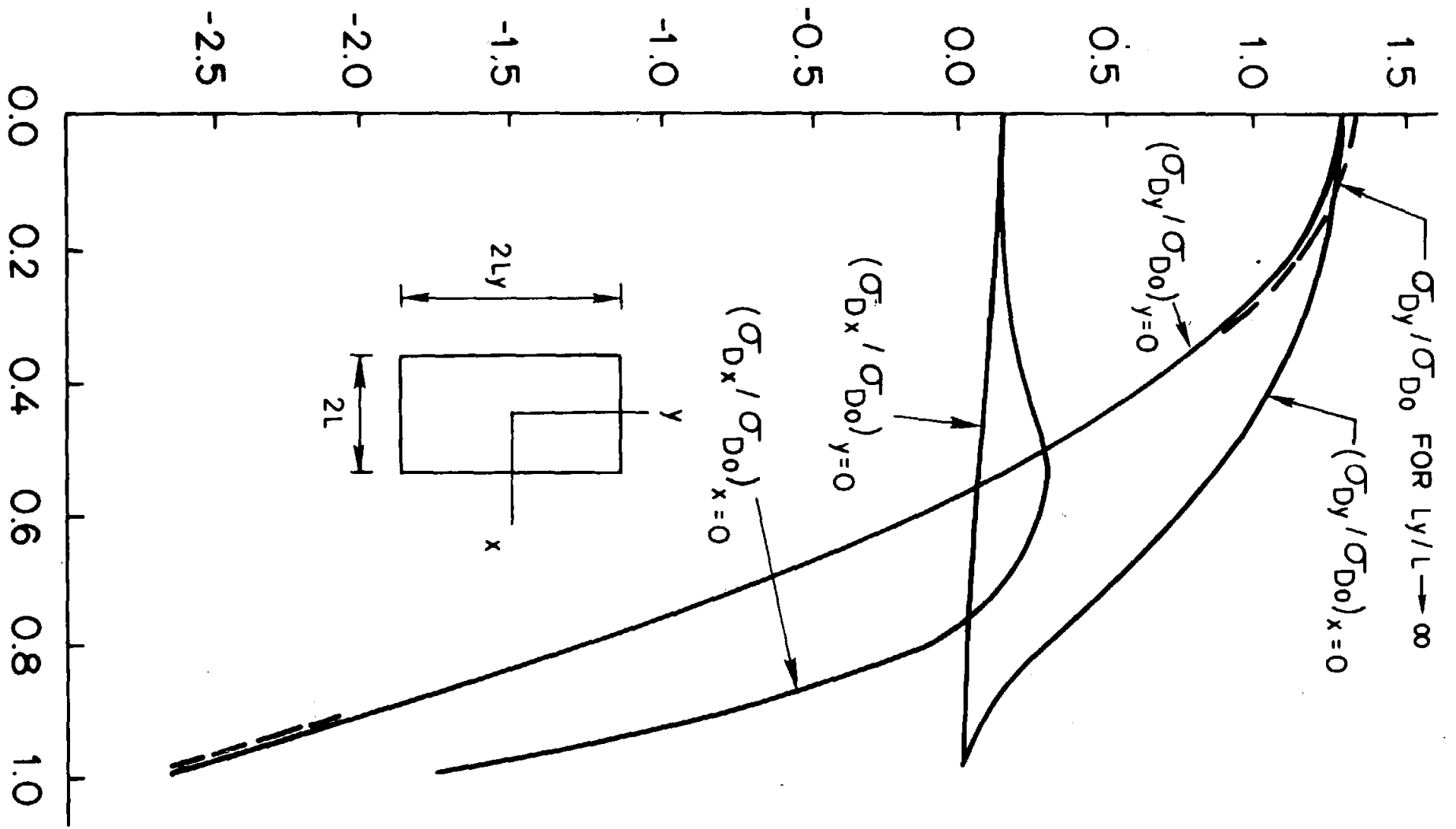

Fig. 3.2 - Variation of residual membrane stresses along axes of symmetry for rectangular plate $L_y/L = 2.0$. The largest component σ_{Dy} is close to that in an infinite plate strip shown by the dashed line. The reference stress is $\sigma_{D0}=EL^2/8R^2$.

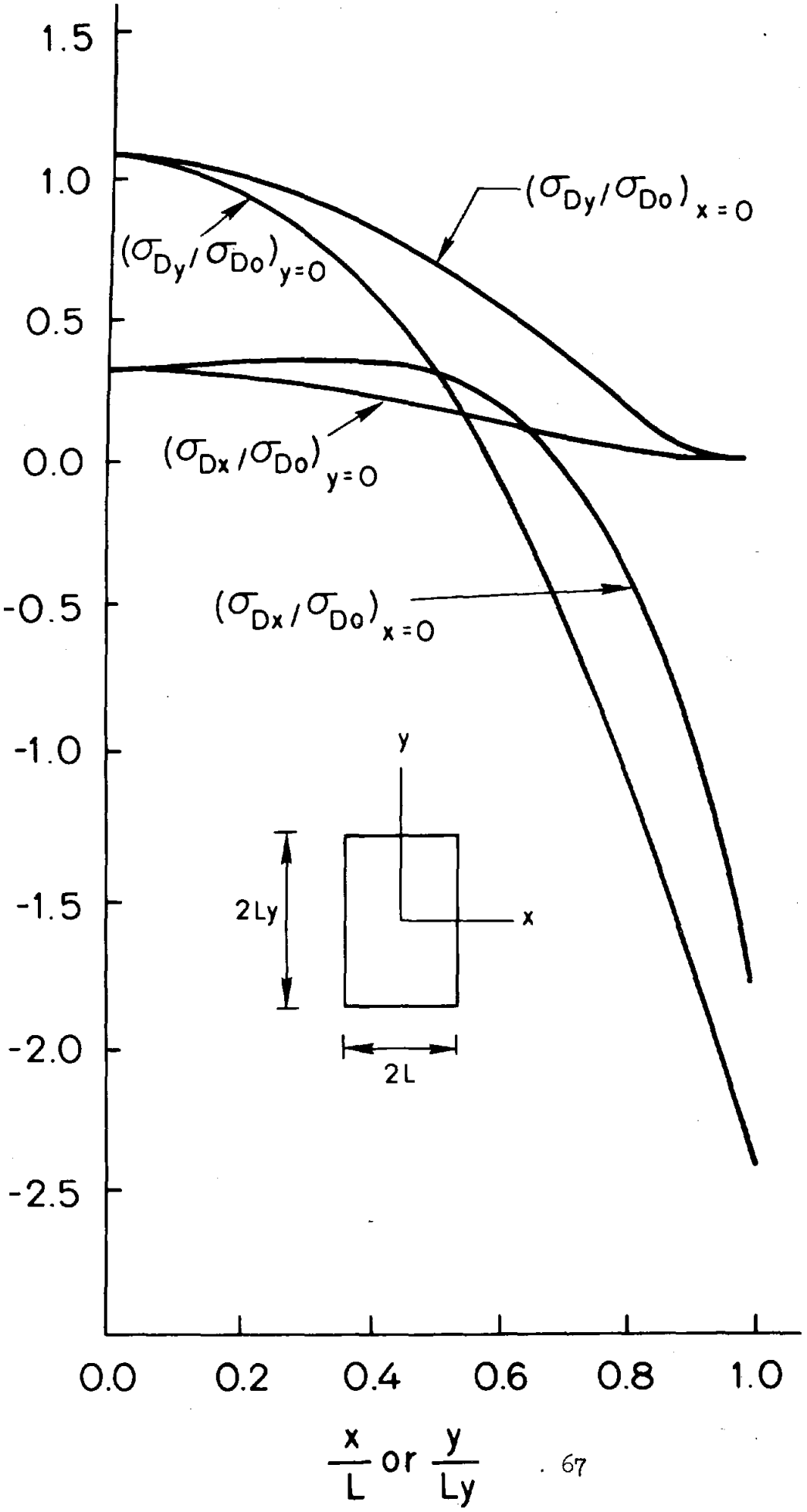

Fig. 3.3 - Membrane stresses in rectangular plate $L_y/L = 1.5$

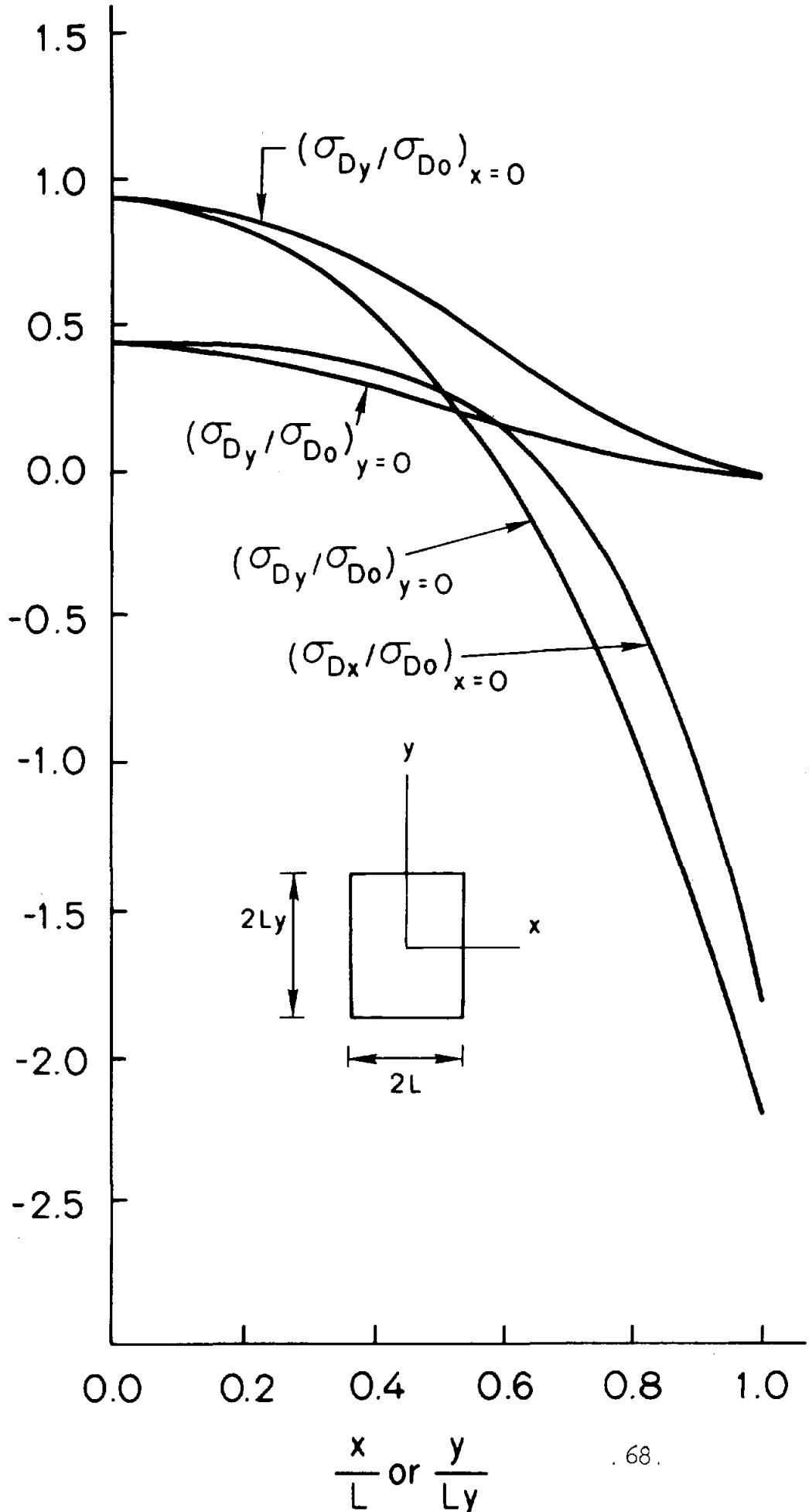

Fig. 3.4 - Membrane stresses in rectangular plate $L_y/L = 1.3$

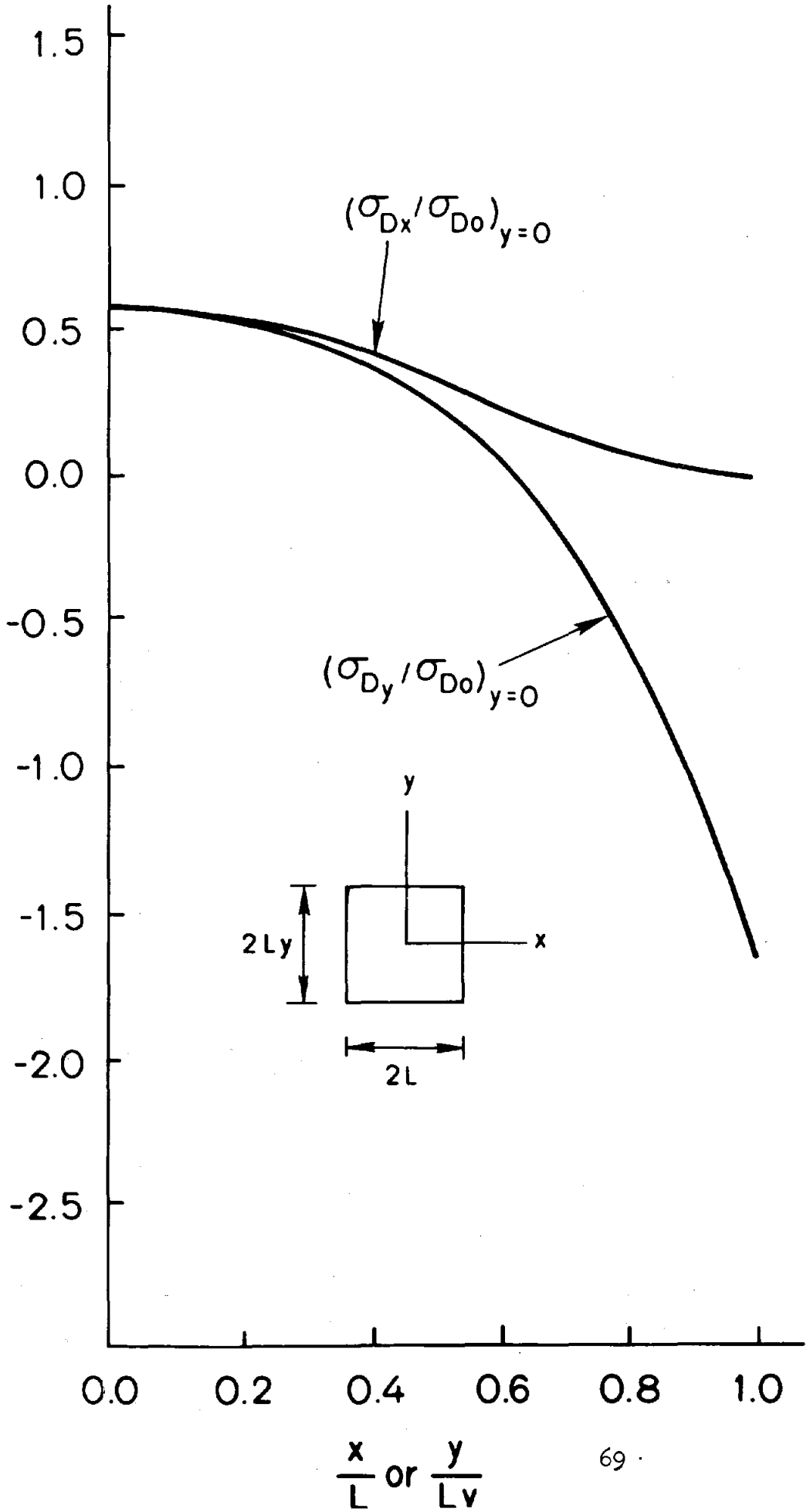

Fig. 3.5 - Variation of membrane stresses in a square plate.

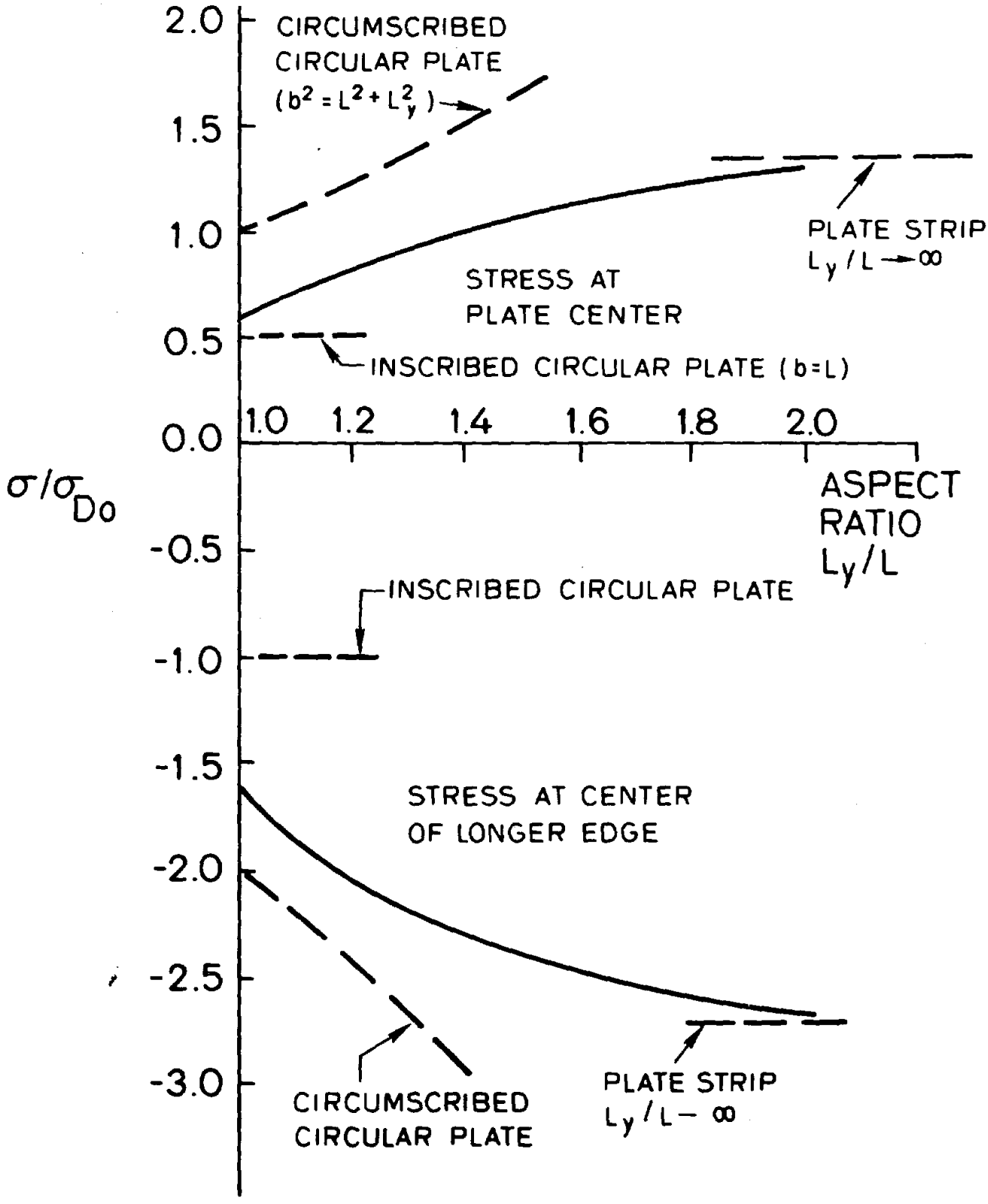

Fig. 3.6 - Variation with aspect ratio of the maximum membrane tensile stresses at the center of the plate, and the maximum membrane compressive stress at the center of the longer edge. Values for the plate strip and circular plates are also shown.

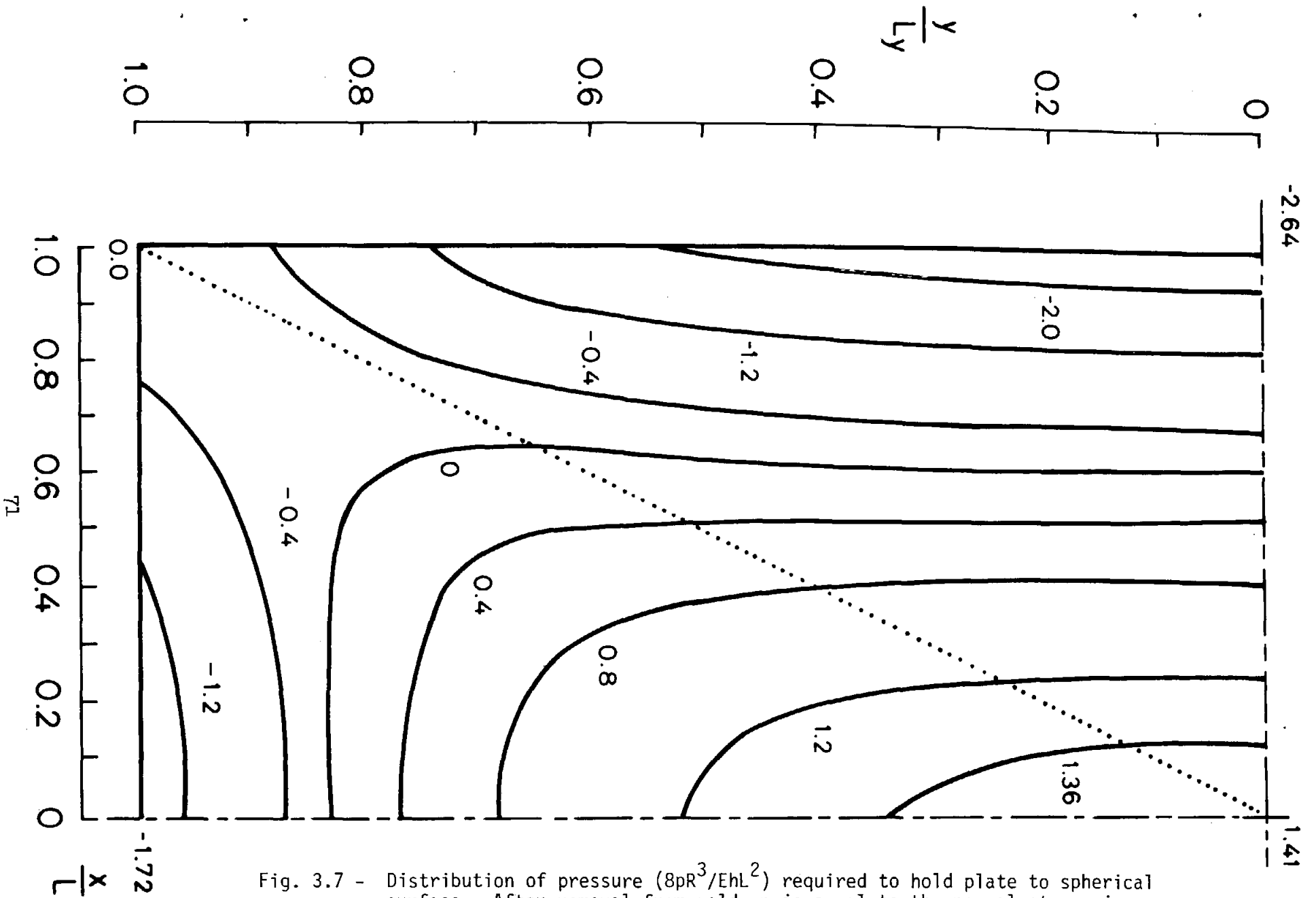

Fig. 3.7 - Distribution of pressure ($8pR^3/EhL^2$) required to hold plate to spherical surface. After removal from mold, p is equal to the normal stress in the adhesive layer between plate and honeycomb, tensile in the center region and compressive in the outer region $L_y/L = 2$.

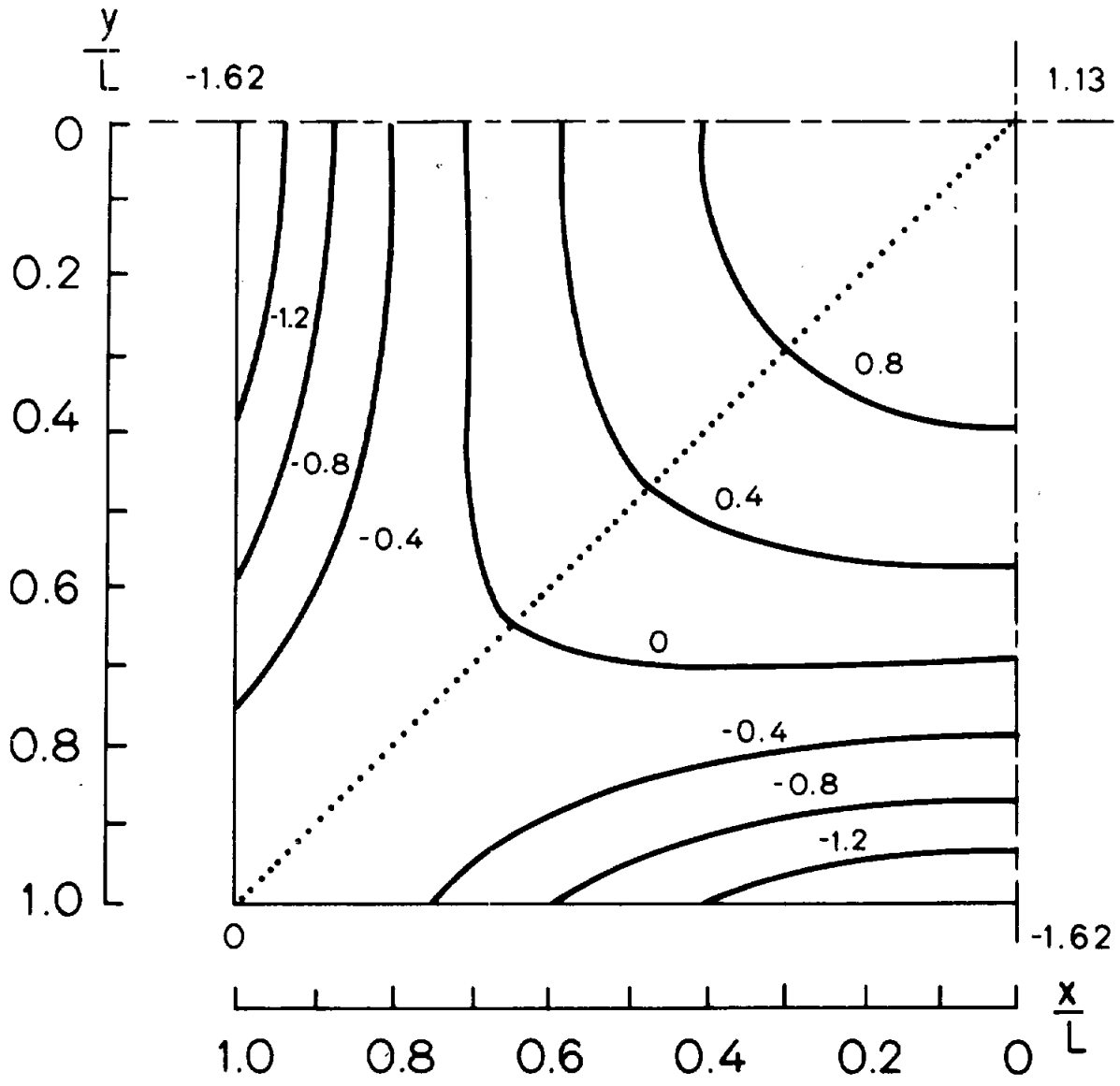

Fig. 3.9 - Pressure as in Fig. 3.7. For square plate L_y=L.

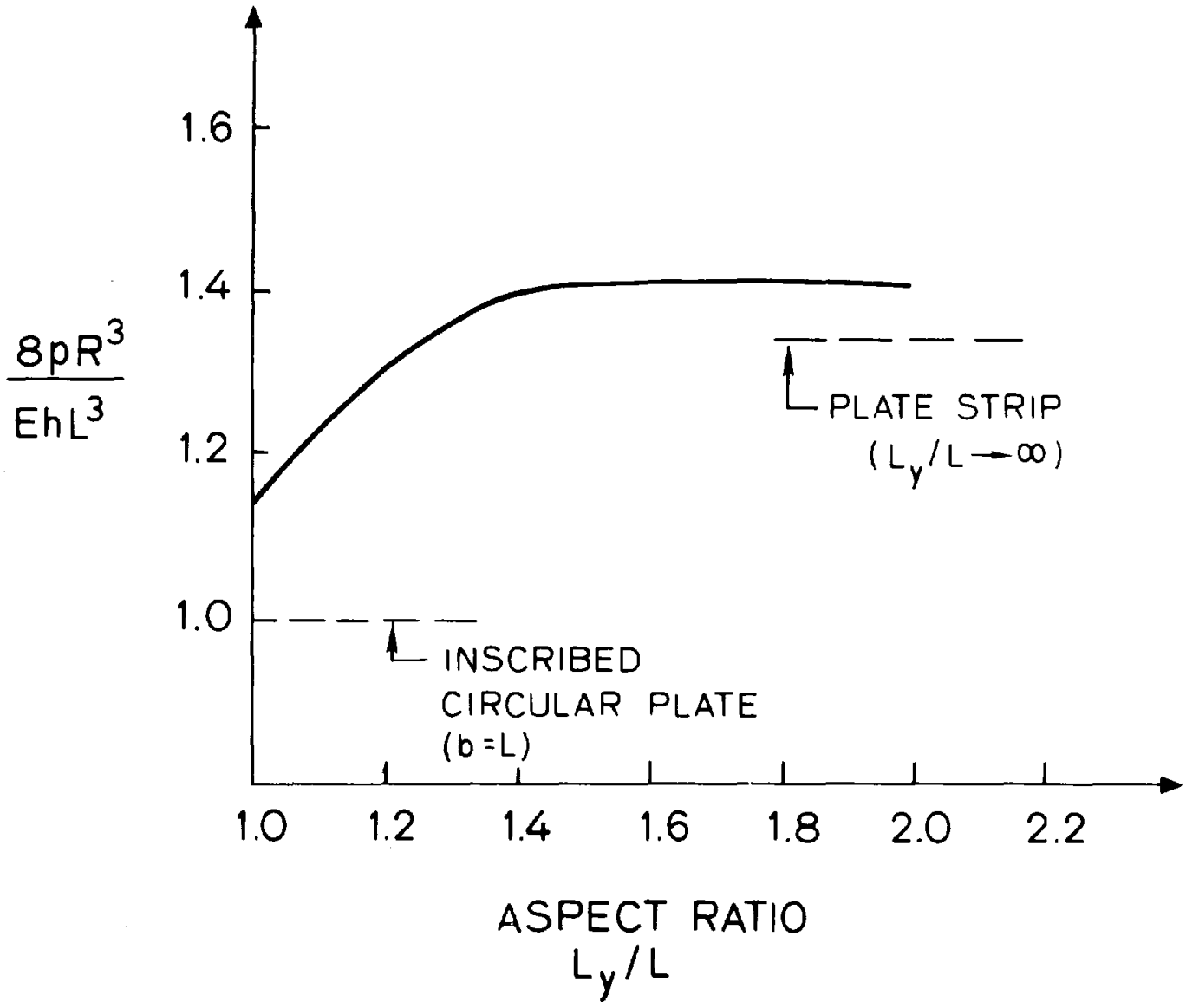

Fig. 3.10 - Variation of pressure at plate center with aspect ratio. After removal from mold, this pressure is the maximum tension in the bond between glass plate and honeycomb (except near the edges).

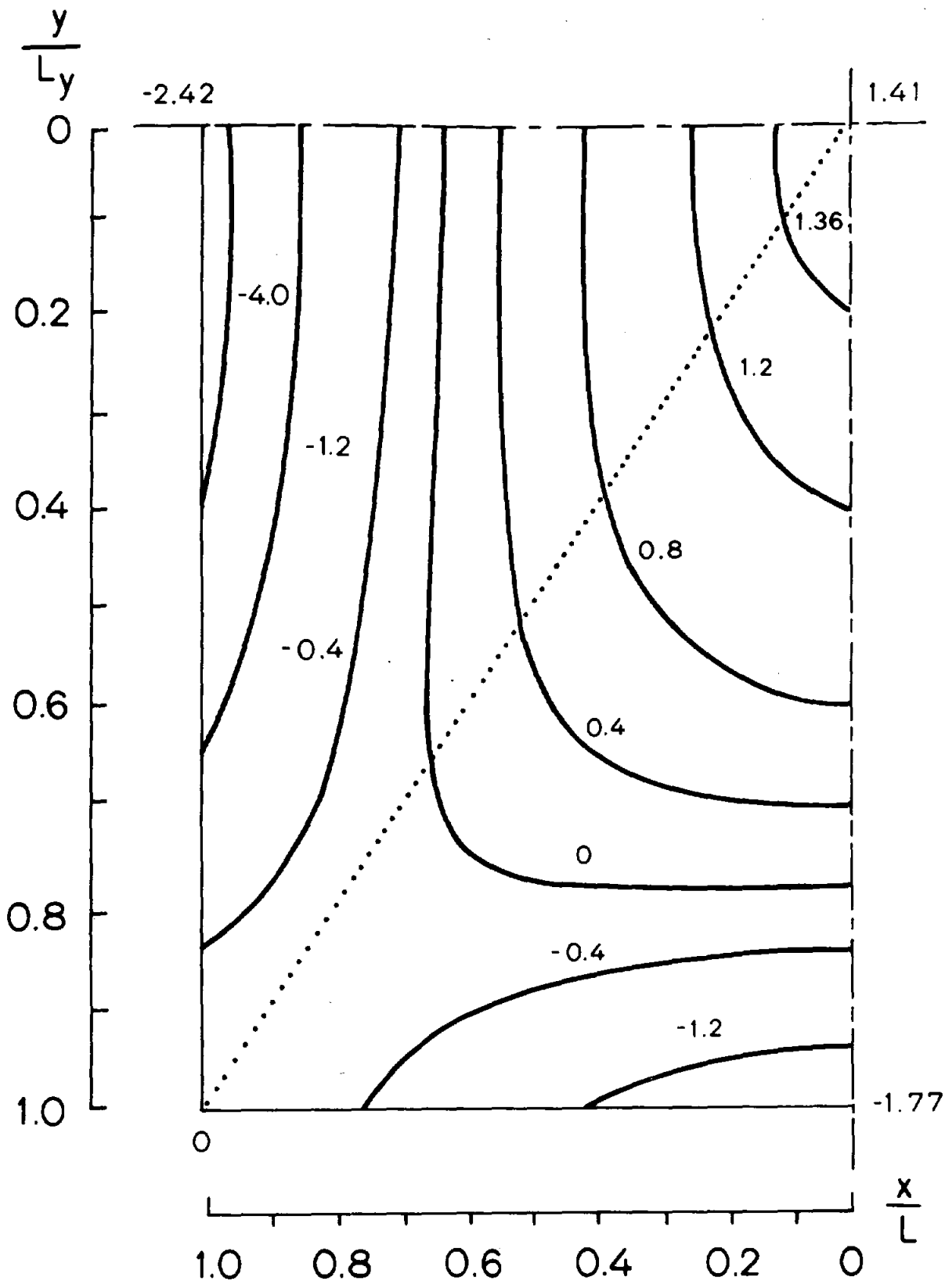

Fig. 3.8 - Pressure as in Fig. 3.7, for $L_y/L = 1.5$

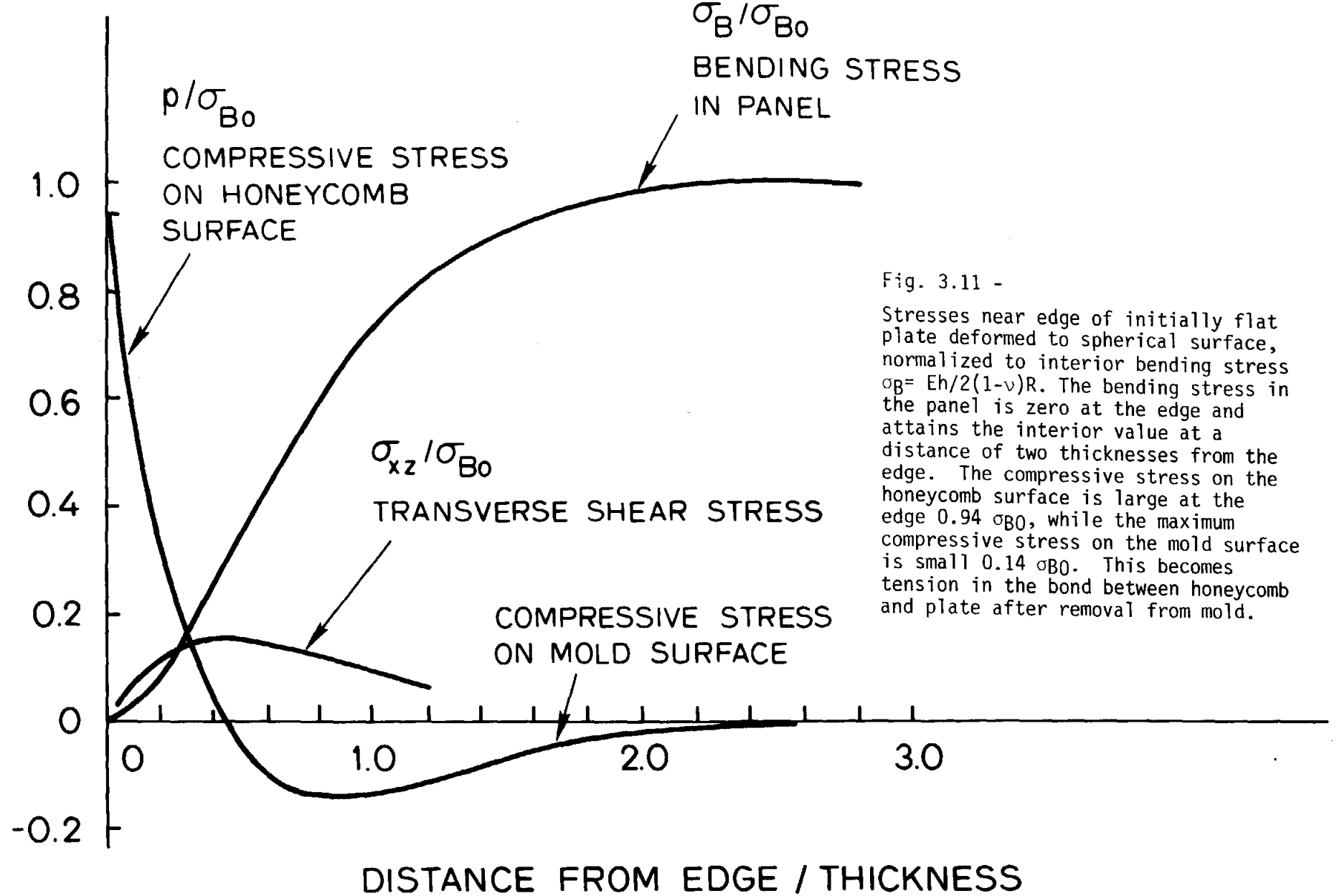

Fig. 3.11 -

Stresses near edge of initially flat plate deformed to spherical surface, normalized to interior bending stress $\sigma_B = Eh/2(1-\nu)R$. The bending stress in the panel is zero at the edge and attains the interior value at a distance of two thicknesses from the edge. The compressive stress on the honeycomb surface is large at the edge 0.94 σ_{BO}, while the maximum compressive stress on the mold surface is small 0.14 σ_{BO}. This becomes tension in the bond between honeycomb and plate after removal from mold.

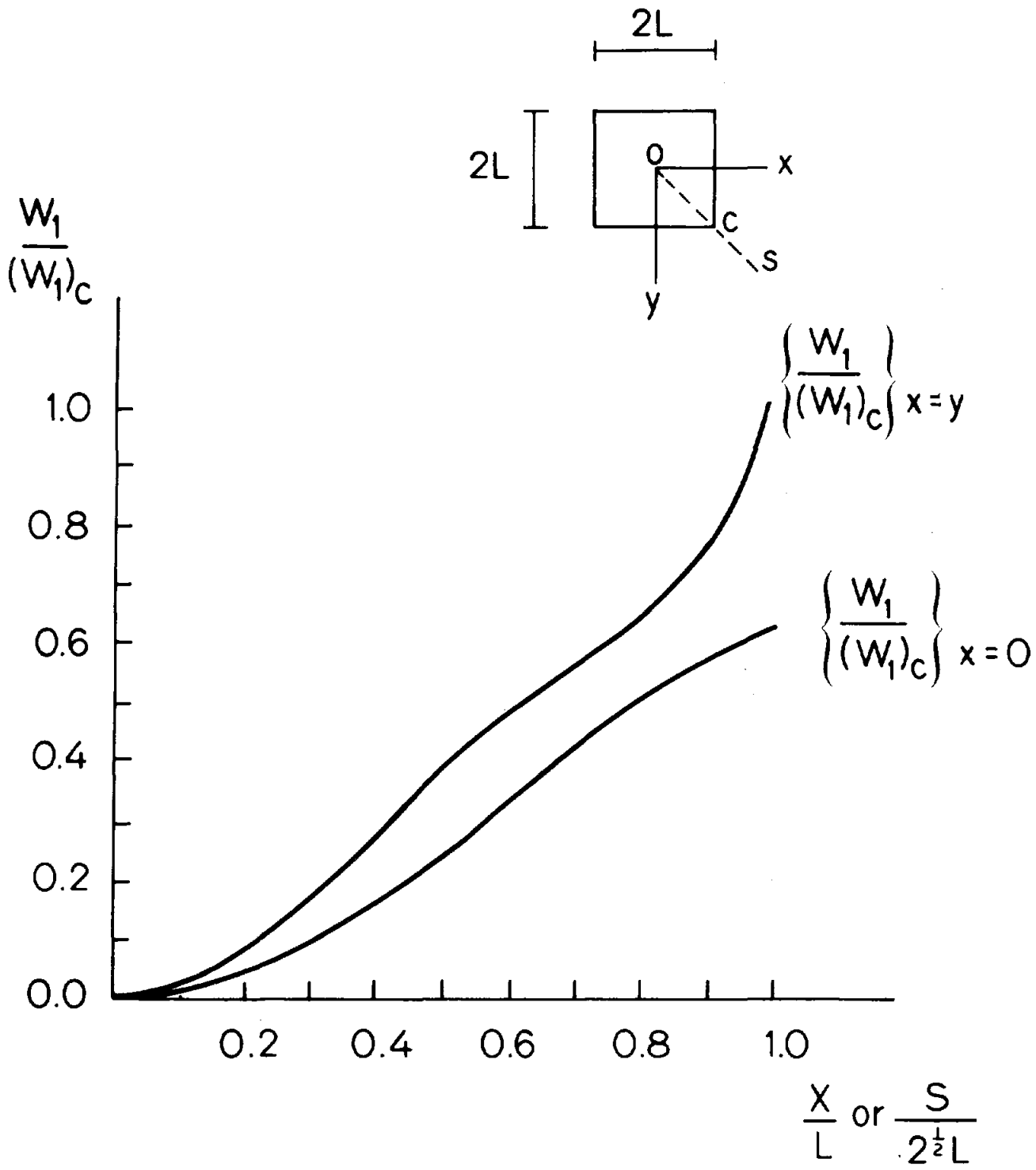

Fig. 4.1 - Elastic springback displacement for square panel. Maximum displacement is at the corner $(w_1)_c = 1.02\ \beta_{10}\ L$

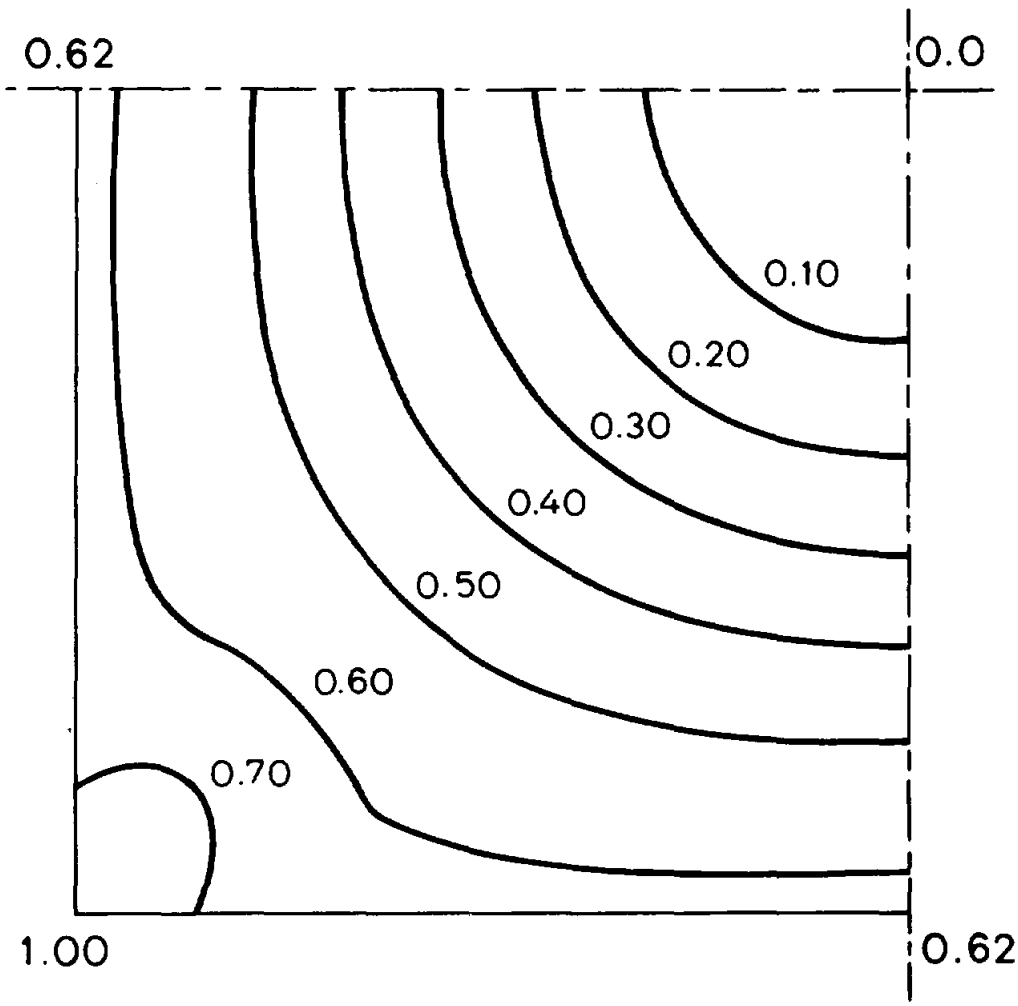

Fig. 4.2 - Contours of constant elastic springback displacement for square panel, normalized to the corner displacement $(w_1)_c = 1.02\ \beta_{10}\ L$.

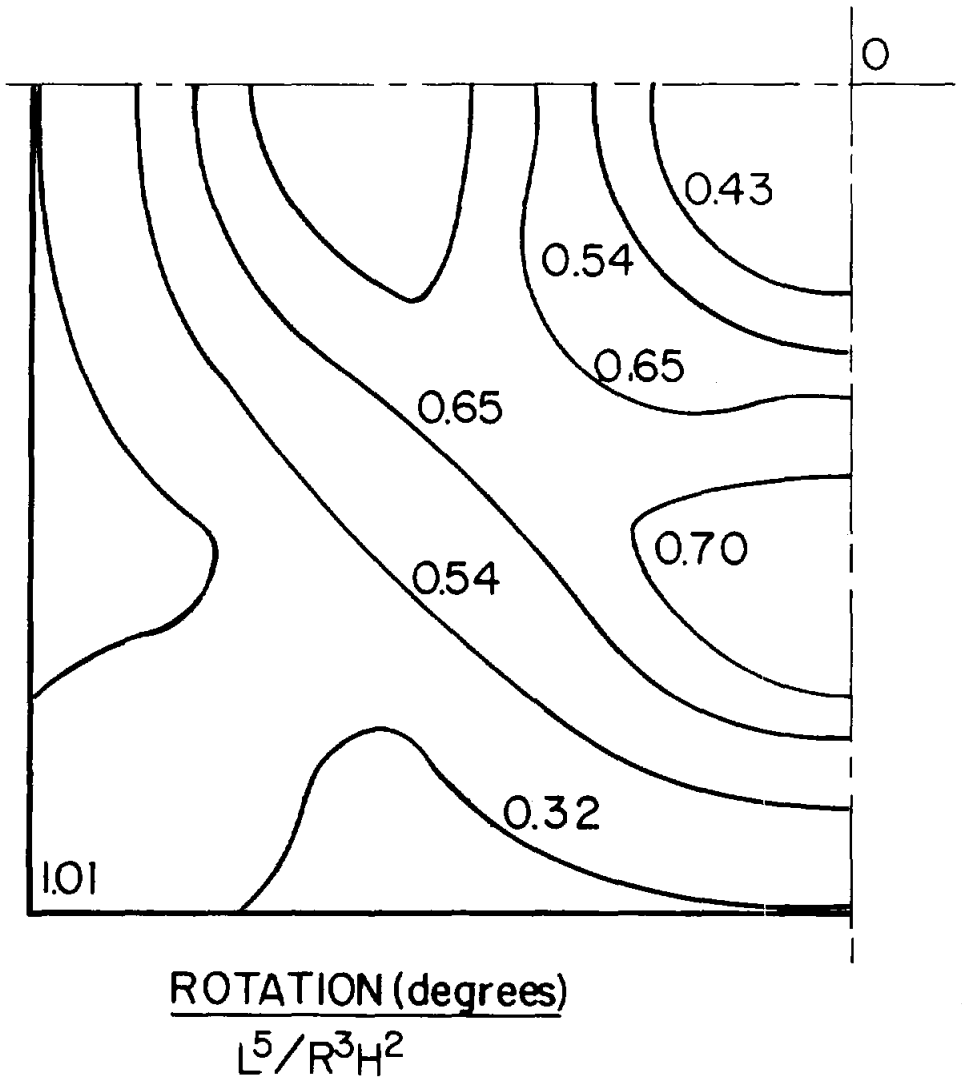

Fig. 4.3 - Contour plot of elastic springback angular deviation of the normal to the square panel surface upon removal from mold. The maximum occurs at the corner and is of the magnitude $ROT^o = 1.01\ L^5/R^3H^2$.

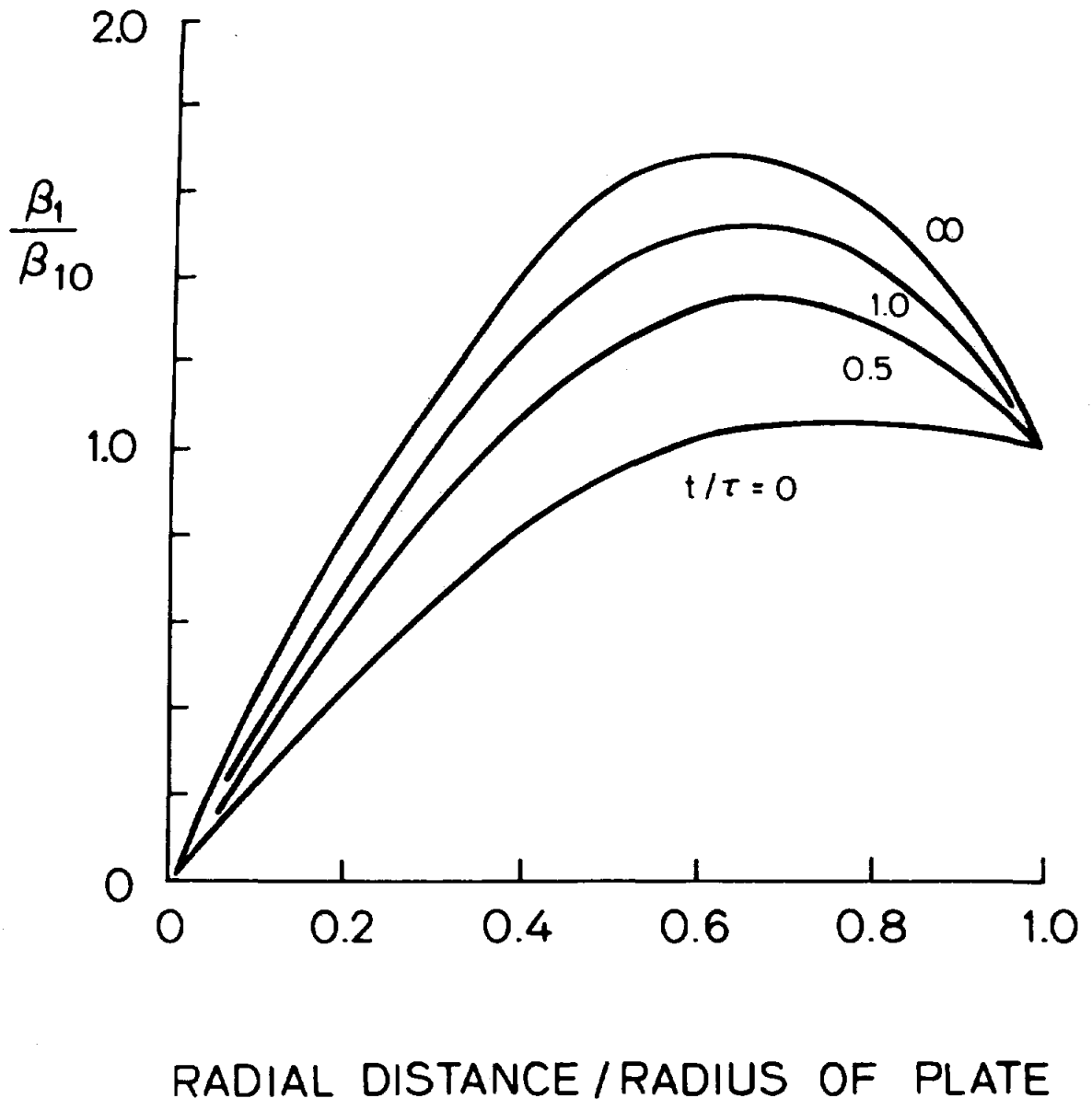

Fig. 4.4 - Deviation of angle of normal from spherical due to springback of panel with viscoelastic core (γ = 2.0).

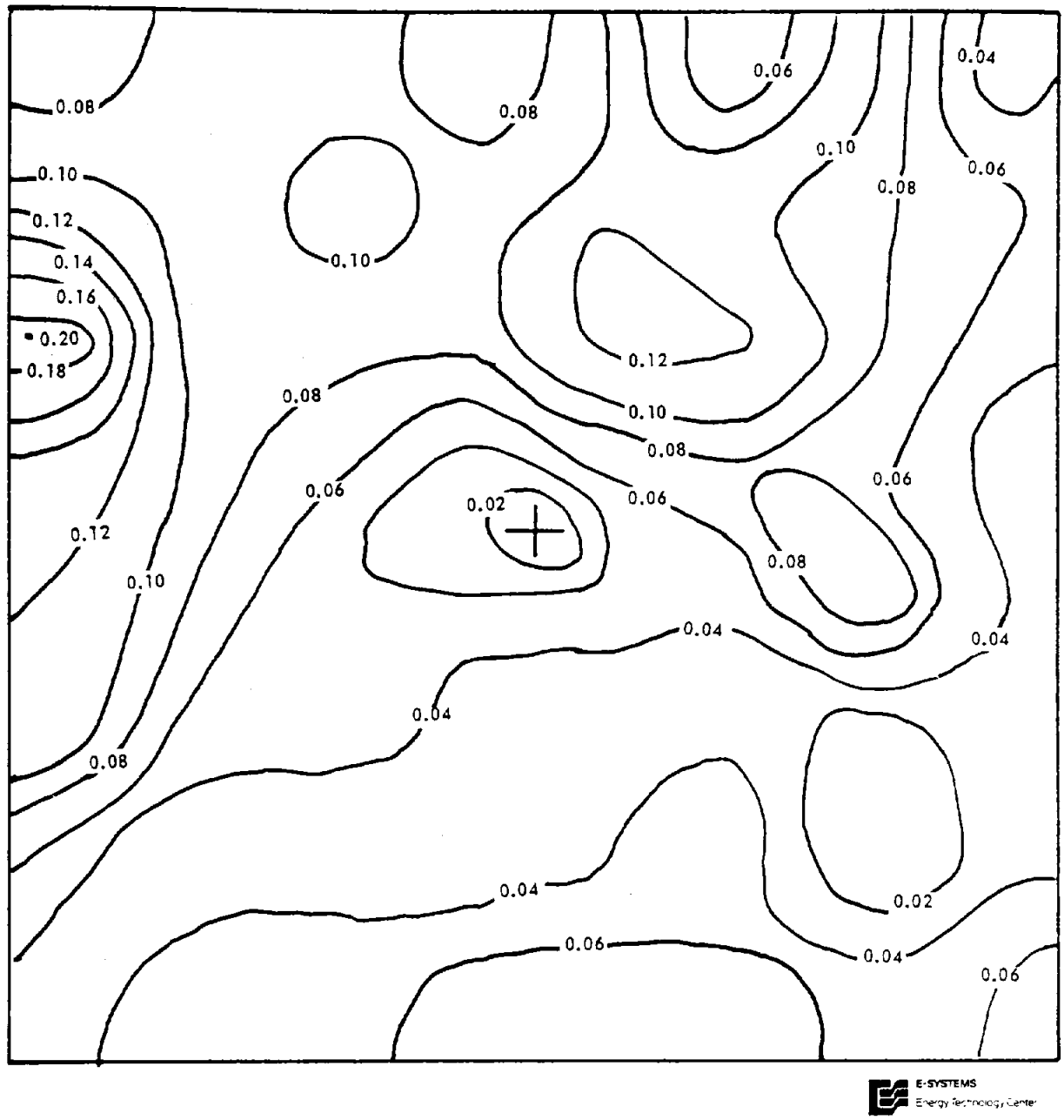

Fig. 4.5 - Contour plot of mirror panel angular deviations (in degrees) for Panel No. 20 (from Perry, 1980)

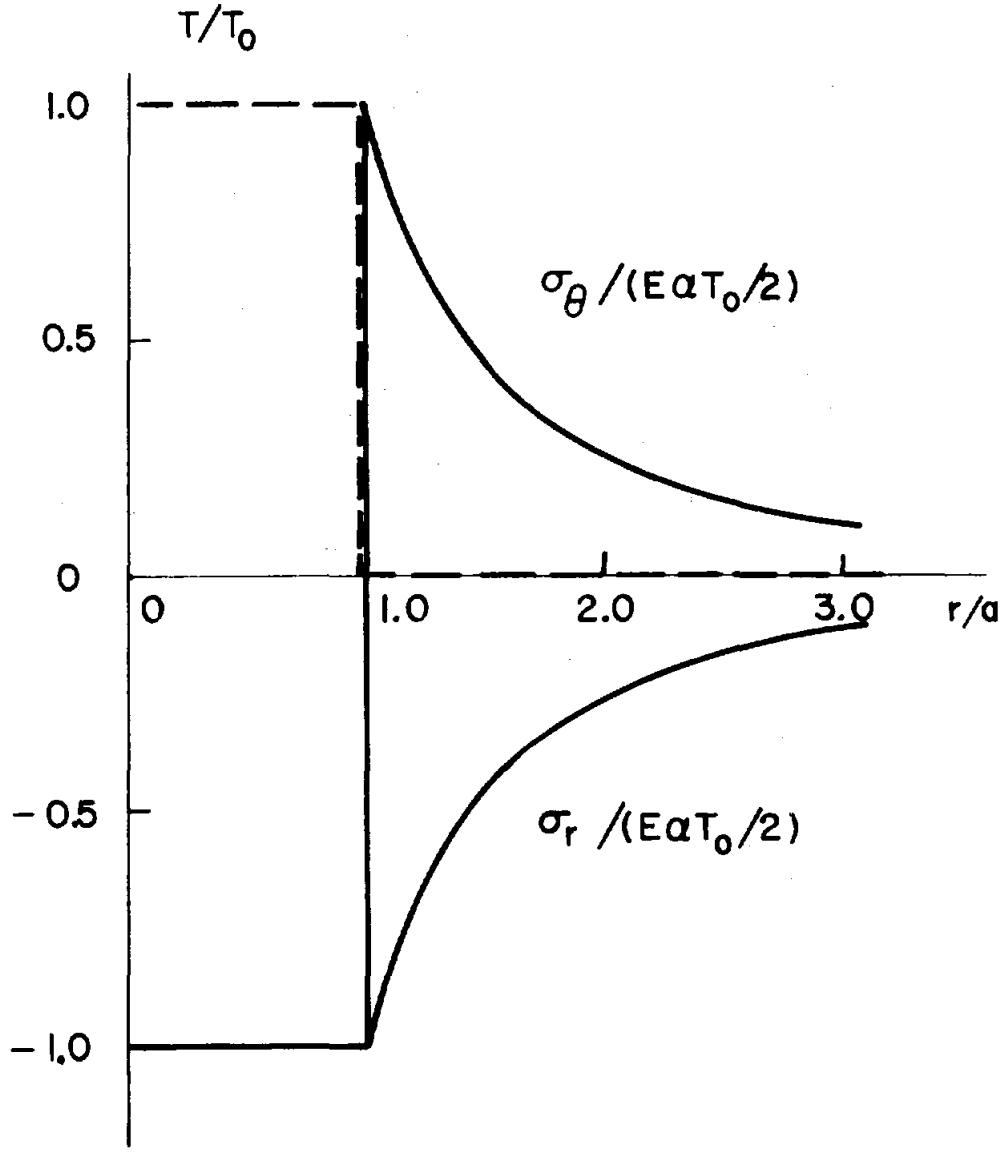

Fig. 5.1 - Stress in an elastic plate due to spot of radius a heated to temperature T_o. Peak tension σ_θ occurs in circumferential direction at edge of hot spot.

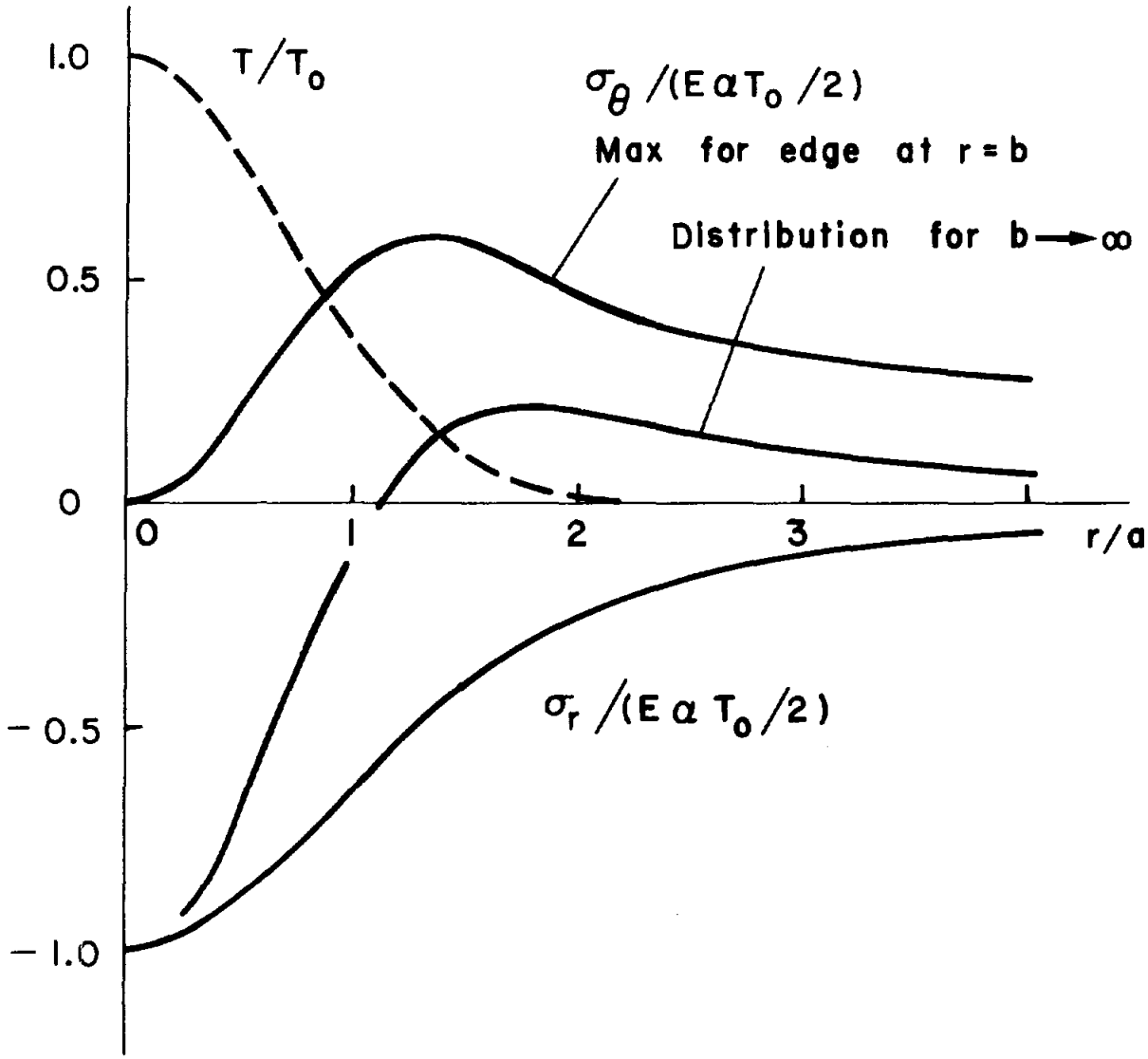

Fig. 5.2 - Stress in an elastic plate due to a heated region with temperature distribution $T = T_0 \exp(-(r/a)^2)$. For the same maximum temperature T_0, the maximum circumferential tension is 21.8% of that for a spot of uniform temperature shown in Fig. 5.1. A free edge at r=b increases the maximum circumferential tension, which has the highest value $\sigma_\theta = 0.30\ E\alpha T_0$.

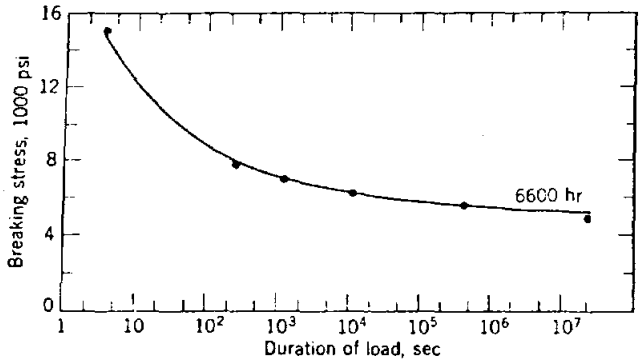

Fig. 6.1 - Strength-time behavior of annealed soda-lime glass rods tested in bending.

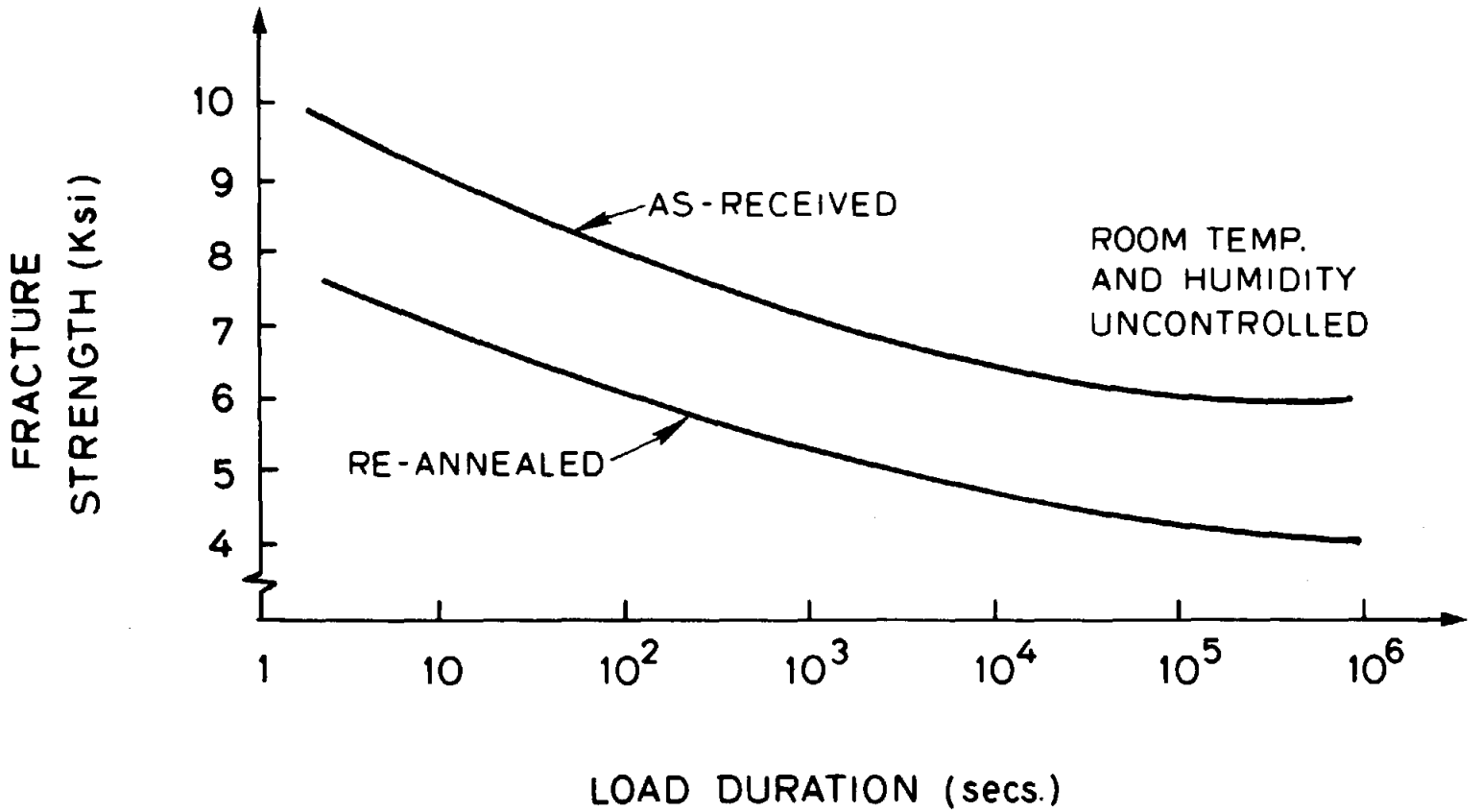

Fig. 6.2 - Strength-time behavior of soda-lime glass specimens tested in bending and containing .002 in. deep surface flaws (semi-circular).

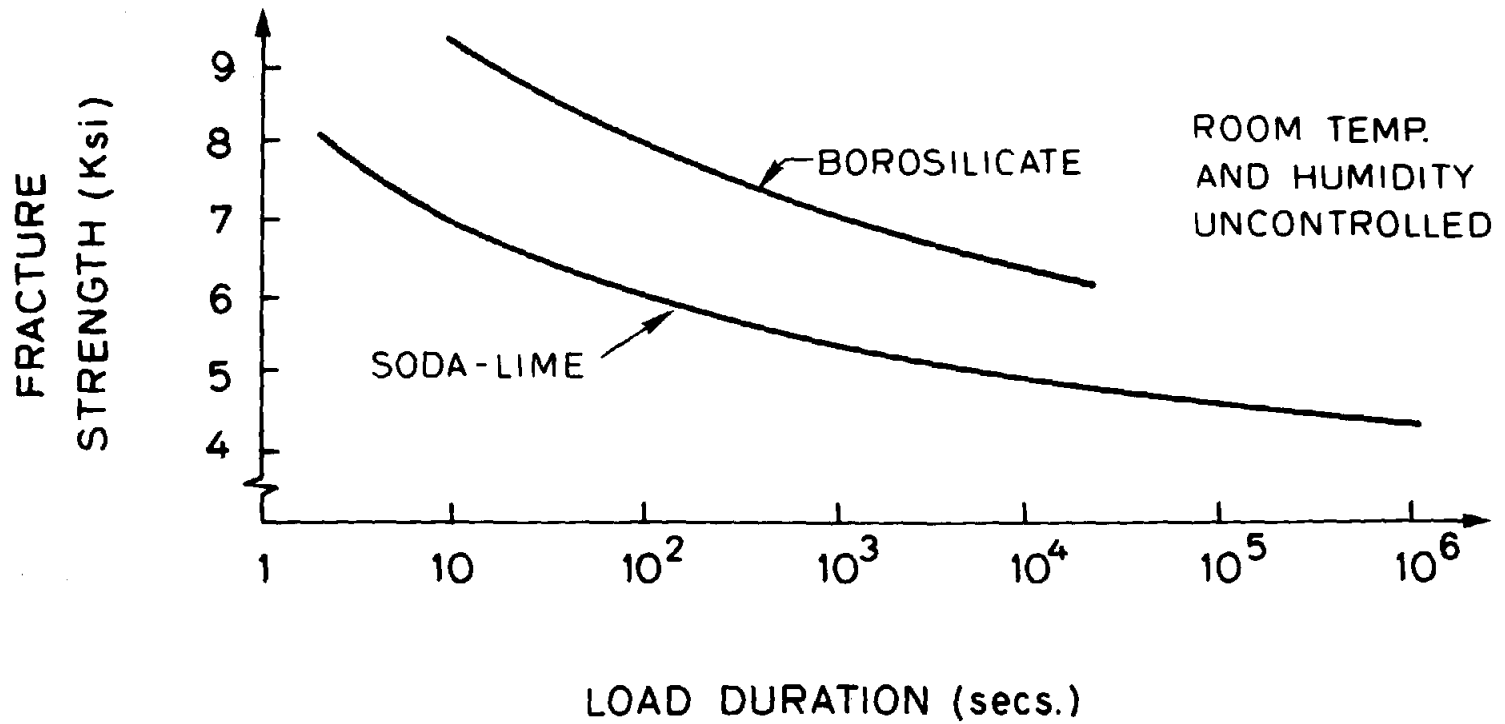

Fig. 6.3 - Comparison of strength-time behavior of annealed soda-lime and borosilicate glasses for the same test conditions as in Fig. 6.2.

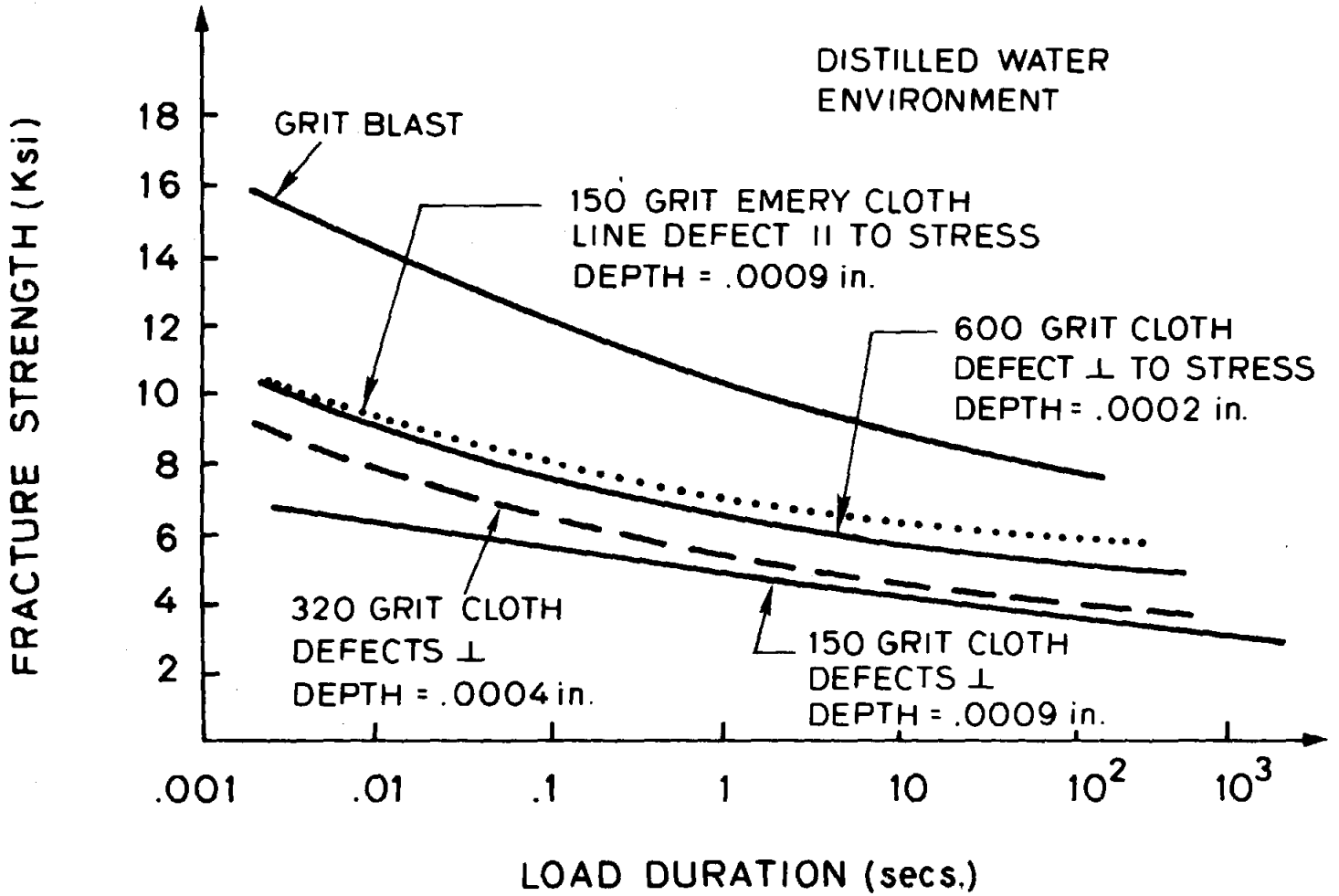

Fig. 6.4 - Strength-time behavior of annealed soda-lime glass specimens tested in bending and containing various initial defects.

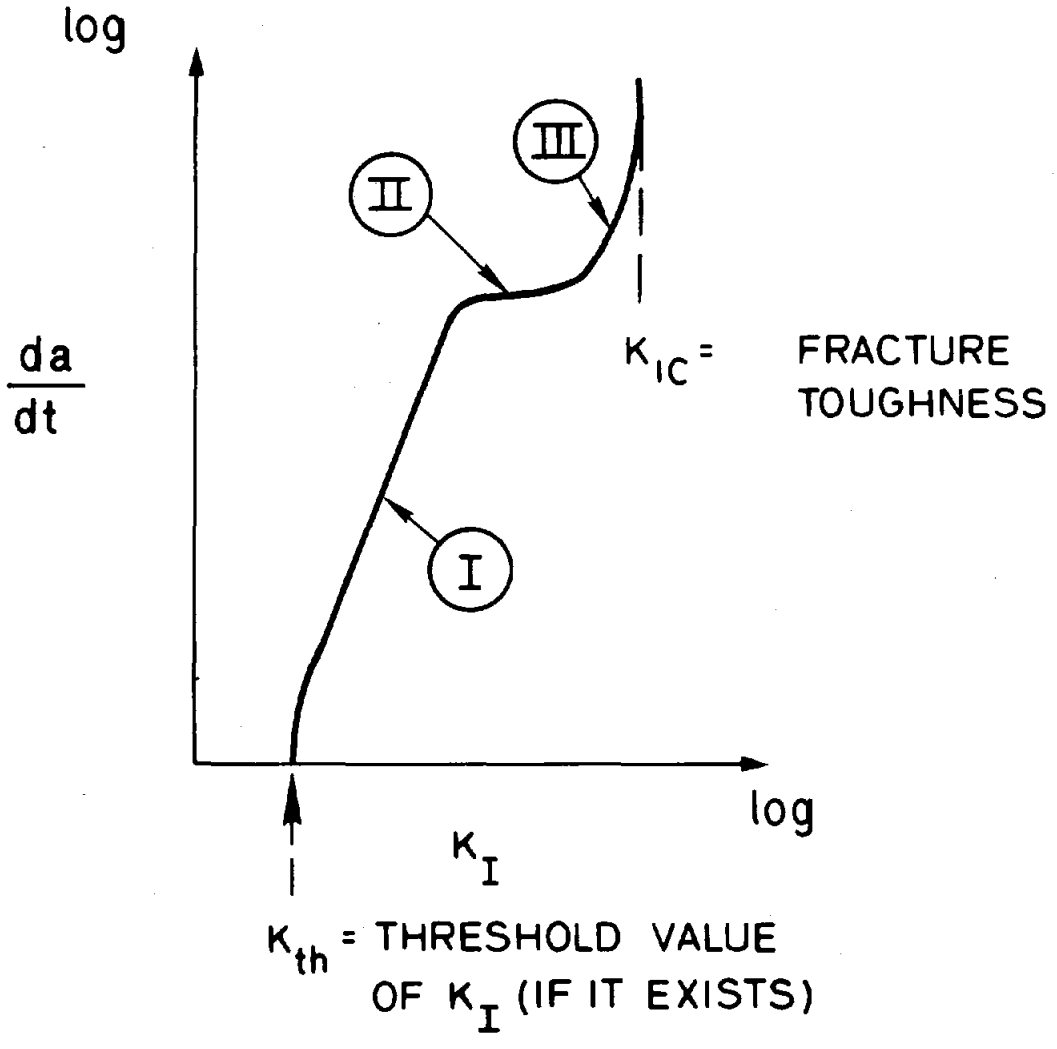

Fig. 6.5 - Schematic of stress corrosion crack growth rate in glass as correlated by the mode I stress intensity factor.

TID 4500 - R66, UC62 (301)

AAI Corporation
P. O. Box 6787
Baltimore, MD 21204

Acurex Aerotherm
485 Clyde Avenue
Mountain View, CA 94042
Attn: J. Vindum

Advanco Corporation
999 N. Sepulveda Blvd.
Suite 314
El Segundo, CA 90245
Attn: B. J. Washom

Alpha Solarco
1014 Vine Street
Suite 2230
Cincinnati, OH 45202

American Boa, Inc.
Suite 4907, One World
Trade Center
New York, NY 10048
Attn: R. Brundage

Anaconda Metal Hose Co.
698 South Main Street
Waterbury, CT 06720
Attn: W. Genshino

Applied Concepts Corp.
P. O. Box 2760
Reston, VA 22090
Attn: J. S. Hauger

Applied Solar Resources
490 East Pima
Phoenix, AZ 85004
Attn: W. H. Coady

Arizona Public Service Co.
Box 21666 MS 1795
Phoenix, AZ 85036
Attn: Dr. B. L. Broussard

Argonne National Laboratory (3)
9700 South Cass Avenue
Argonne, IL 60439
Attn: K. Reed
W. W. Schertz
R. Winston

BDM Corporation
1801 Randolf Street
Albuquerque, NM 87106
Attn: T. Reynolds

Battelle Memorial Institute
Pacific Northwest Laboratory
P. O. Box 999
Richland, WA 99352
Attn: K. Drumheller

Bechtel National, Inc.
P. O. Box 3965
50 Beale Street
San Francisco, CA 94119
Attn: E. Y. Lam

Black and Veatch (2)
P. O. Box 8405
Kansas City, MO 64114
Attn: Dr. J. C. Grosskreutz
D. C. Gray

Boeing Space Center (2)
M/S 86-01
Kent, WA 98131
Attn: S. Duzick
A. Lunde

Boomer-Fiske, Inc.
4000 S. Princeton
Chicago, IL 60609
Attn: C. Cain

Budd Company
Fort Washington, PA 19034
Attn: W. W. Dickhart

Budd Company (The)
Plastic R&D Center
356 Executive Drive
Troy, MI 48084
Attn: J. N. Epel

Burns & Roe (2)
185 Crossways Park Dr.
Woodbury, NY 11797
Attn: R. J. Vondrasket
J. Wysocki

Carrier Corp.
Energy Systems Div.
Summit Landing
P. O. Box 4895
Syracuse, NY 13221
Attn: R. A. English

Compudrive Corp.
76 Treble Core Road
N. Billerica, MA 01862
Attn: T. Black

Cone Drive
Division of Excello Corp.
P. O. Box 272
240 E. 12th Street
Traverse City, MI 49684
Attn: J. E. McGuire

Congressional Research Service
Library of Congress
Washington, DC 20540
Attn: H. Bullis

Corning Glass Company
Corning, NY 14830
Attn: A. F. Shoemaker
W. Baldwin

Custom Engineering, Inc.
2805 South Tejon Street
Englewood, CO 80110
Attn: C. A. de Moraes

DSET
Black Canyon Stage
P. O. Box 185
Phoenix, AZ 85029
Attn: G. A. Zerlaut

Del Manufacturing Co.
905 Monterey Pass Road
Monterey Park, CA 91754
Attn: M. M. Delgado

Desert Research Inst. Energy
Systems Laboratory
1500 Buchanan Blvd.
Boulder City, NV 89005
Attn: J. O. Bradley

Donnelly Mirrors, Inc.
49 West Third Street
Holland, MI 49423
Attn: J. A. Knister

Easton Utilities Commission
219 North Washington Street
Easton, MN 21601
Attn: W. H. Corkran, Jr.

Eaton Corporation
Industrial Drives Operations
Cleveland Division
3249 East 80th St.
Cleveland, OH 44104
Attn: R. Glatt

Edison Electric Institute
90 Park Avenue
New York, NY 10016
Attn: L. O. Elsaesser

Electric Power Research
Institute (2)
3412 Hillview Avenue
Palo Alto, CA 94303
Attn: Dr. J. Cummings
J. E. Bigger

Energetics
833 E. Arapahoe Street
Suite 202
Richardson, TX 85081
Attn: G. Bond

Energy Institute
1700 Las Lomas NE
Albuquerque, NM 87131

E-Systems, Inc.
Energy Tech. Center
P. O. Box 226118
Dallas, TX 75266
Attn: R. R. Walters

Eurodrive, Inc.
2001 W. Main St.
Troy, OH 45373
Attn: S. D. Warner

Exxon Enterprises (3)
P. O. Box 592
Florham Park, NJ 07923
Attn: J. Hamilton
P. Joy
Dr. M. C. Noland

Florida Solar Energy Center (2)
300 State Road, Suite 401
Cape Canaveral, FL 32920
Attn: C. Beech
D. Block

Ford Aerospace and Comm.
3939 Fabian Way
Palo Alto, CA 94303
Attn: H. H. Sund

Ford Glass Division
Glass Technical Center
25500 West Outer Drive
Lincoln Park, MI 48246
Attn: H. A. Hill

General Atomic
P. O. Box 81608
San Diego, CA 92138
Attn: A. Schwartz

General Electric Co. (2)
P. O. Box 8661
Philadelphia, PA 19101
Attn: W. Pijawka
C. Billingsley

General Motors
Harrison Radiator Division
Lockport, NY 14094
Attn: L. Brock

General Motors Corporation
Technical Center
Warren, MI 48090
Attn: J. F. Britt

Georgia Inst. of Technology
Atlanta, GA 30332
Attn: J. D. Walton

Georgia Power Company
270 Peachtree
P. O. Box 4545
Atlanta, GA 30302
Attn: J. Roberts

Glitsch, Inc.
P. O. Box 226227
Dallas, TX 75266
Attn: R. W. McClain

Haveg Industries, Inc.
1287 E. Imperial Highway
Santa Fe Springs, CA 90670
Attn: J. Flynt

Hexcel
11711 Dublin Blvd.
Dublin, CA 94566
Attn: R. Johnston

Highland Plating
1128 N. Highland
Los Angeles, CA 90038
Attn: M. Faeth

Honeywell, Inc.
Energy Resources Center
2600 Ridgeway Parkway
Minneapolis, MN 55413
Attn: J. R. Williams

Insights West
900 Wilshire Blvd.
Los Angeles, CA 90017
Attn: J. H. Williams

Jacobs Engineering Co.
251 South Lake Avenue
Pasadena, CA 91101
Attn: R. Morton

Jet Propulsion Laboratory (3)
4800 Oak Grove Drive
Pasadena, CA 91103
Attn: J. Becker
J. Lucas
V. C. Truscello

Kingston Industries Corp.
205 Lexington Ave.
New York, NY 10016
Attn: M. Sherwood

Lawrence Livermore Laboratory
University of California
P. O. Box 808
Livermore, CA 94500
Attn: W. C. Dickinson

Los Alamos Scientific Lab. (3)
Los Alamos, NM 87545
Attn: J. D. Balcomb
C. D. Bankston
D. P. Grimmer

McDonnell-Douglas Astronautics Company (3)
5301 Bolsa Avenue
Huntington Beach, CA 92647
Attn: J B. Blackmon
J. Rogan
D. Steinmeyer

Morse Chain
Division of Borg-Warner Corp.
4650 Steele St.
Denver, CO 80211
Attn: G. Fukayama

Motorola, Inc.
Government Electronics Divsion
8201 E. McDowell Road
P. O. Box 1417
Scottsdale, AZ 85252
Attn: R. Kendall

New Mexico State University
Solar Energy Department
Las Cruces, NM 88001

Oak Ridge National Lab (3)
P. O. Box Y
Oak Ridge, TN 37830
Attn: S. I. Kaplan
G. Lawson
W. R. Mixon

Office of Technology Assessment
U. S. Congress
Washington, DC 20510
Attn: R. Rowberg

Omnium G
1815 Orangethorpe Park
Anaheim, CA 92801
Attn: S. P. Lazzara

Owens-Illinois
1020 N. Westwood
Toledo, OH 43614
Attn: Y. K. Pei

PPG Industries, Inc.
One Gateway Center
Pittsburg, PA 15222
Attn: C. R. Frownfelter

PRC Energy Analysis Company
7600 Old Springhouse Road
McLean, VA 22101

Parsons of California
3437 S. Airport Way
Stockton, CA 95206
Attn: D. R. Biddle

Progress Industries, Inc.
7290 Murdy Circle
Huntington Beach, CA 92647
Attn: K. Busche

Ronel Technetics, Inc.
501 West Sheridan Road
McHenry, IL 60050
Attn: N. Wensel

Schott America
11 East 26th St.
New York, NY 10010
Attn: J. Schrauth

Scientific Applications, Inc.
100 Mercantile Commerce Bldg.
Dallas, TX 75201
Attn: Dr. J. W. Doane

Scientific Atlanta, Inc.
3845 Pleasantdale Road
Atlanta, GA 30340
Attn: A. Ferguson

Shelltech Associates (20)
809 Tolman Drive
Stanford, CA 94305
Attn: C. R. Steele

Solar Energy Information Center
1536 Cole Blvd.
Golden, CO 80401
Attn: R. Ortiz

Solar Energy Research Institiute (1
1536 Cole Blvd.
Golden, CO 80401
Attn: B. L. Butler
L. G. Dunham (4)
B. P. Gupta
F. Kreith
J. Thornton
K. Touryan
N. Woodley
D. W. Kearney
C. Bishop
B. Feasby

Solar Energy Technology
Rocketdyne Division
6633 Canoga Avenue
Canoga Park, CA 91304
Attn: Jim Friefield

Solar Kinetics, Inc.
P. O. Box 47045
8120 Chancellor Row
Dallas, TX 75247
Attn: G. Hutchison

Southwest Research Institute
P. O. Box 28510
San Antonio, TX 78284
Attn: D. M. Deffenbaugh

Stanford Research Institute
Menlo Park, CA 94025
Attn: A. J. Slemmons

Stearns-Rogers
4500 Cherry Creek
Denver, CO 80217
Attn: W. R. Lang

W. B. Stine
317 Monterey Rd., Apt. 22
South Pasadena, CA 91303

Sun Gas Company
Suite 800, 2 N. Park E
Dallas, TX 75231
Attn: R. C. Clark

Sun Heet, Inc.
2624 S. Zuni
Englewood, CO 80110

Sunpower Systems
510 S. 52 Street
Tempe, AZ 85281
Attn: W. Matlock

Sundstrand Electric Power
4747 Harrison Avenue
Rockford, IL 61101
Attn: A. W. Adam

Suntec Systems, Inc.
2101 Wooddale Drive
St. Paul, MN 55110
Attn: L. W. Rees

Sweedlow, Inc.
12122 Western Avenue
Garden Grove, CA 92645
Attn: E. Nixon

3M-Decorative Products Div.
209-2N 3M Center
St. Paul, MN 55101
Attn: B. Benson

3M-Product Development
Energy Control Products
207-1W 3M Center
St. Paul, MN 55101
Attn: J. R. Roche

TRW, Inc.
Energy Systems Group of TRW, Inc.
One Space Park, Bldg. R4, Rm. 2074
Redondo Beach, CA 90278
Attn: J. M. Cherne

Team, Inc.
120 West Broadway, No. 41
Tucson, AZ 85701
Attn: Roger Harwell

Texas Tech University
Dept. of Electrical Engineering
P. O. Box 4709
Lubbock, TX 79409
Attn: J. D. Reichert

Toltec Industries, Inc.
40th and East Main
Clear Lake, IA 50428
Attn: D. Chenault

U. S. Department of Energy (3)
Albuquerque Operations Office
P. O. Box 5400
Albuquerque, NM 87185
Attn: G. N. Pappas
J. A. Morley
J. Weisiger

U. S. Department of Energy
Div. of Energy Storage Systems
Washington, DC 20545
Attn: J. Gahimer

U. S. Department of Energy (8)
Solar Thermal Energy Sys. Div.
Washington, DC 20585
Attn: W. W. Auer
G. W. Braun
J. E. Greyerbiehl
M. U. Gutstein
L. Melamed
J. E. Rannels
F. Wilkins
J. Dollard

U. S. Department of Energy (2)
San Francisco Operations Office
1333 Broadway, Wells Fargo Bldg.
Oakland, CA 94612
Attn: R. W. Hughey

University of Kansas Center for
Reserch, CRINC
2291 Irving Hall Rd.
Lawrence, KS 66045
Attn: R. F. Riordan

University of New Mexico (2)
Department of Mechanical Eng.
Albuquerque, NM 87113
Attn: M. W. Wilden
W. A. Cross

Viking
3467 Ocean View Blvd.
Glendale, CA 91208
Attn: G. Guranson

Winsmith
Div. of UMC Industries, Inc.
Springville, NY 14141
Attn: R. Bhise

Wyle Lab
7800 Governor's Drive West
Huntsville, AL 35807
Attn: R. Losey

1520 T. J. Hoban
1530 W. E Caldes
1550 F. W. Neilson
2320 K. L. Gillespie
2323 C. M. Gabriel
2324 R. S. Pinkham
2326 G. M. Heck
3161 J. E. Mitchell
3600 R. W. Hunnicutt
Attn: H. H. Pastorius, 3640
3700 J. C. Strassel
4000 A. Narath
4231 J. H. Renken
4700 J. H. Scott
4710 G. E. Brandvold (10)
4713 B. W. Marshall
4714 R. P. Stromberg (20)
4715 R. H. Braasch
4716 J. F. Banas
4717 E. L. Harley
4717 J. A. Leonard
4720 J. H. Scott
4721 J. V. Otts
4723 W. P. Schimmel
4724 D. G. Schueler
4726 E. Burgess
4750 V. L. Dugan
5510 D. B. Hayes
5513 D. W. Larson
5520 T. B. Lane
5523 R. C. Reuter
5810 R. G. Kepler
5820 R. E. Whan
5830 M. J. Davis
5833 J. L. Jellison
5840 N. Magnani
8214 M. A. Pound
8450 R. C. Wayne
8451 C. F. Melius
8451 W. R. Delameter
8452 A. C. Skinrood
8452 T. Bramlette
8453 W. G. Wilson
3141 J. L. Erickson (5)
3151 W. L. Garner (3)
(Unlimited Release)
For DOE/TIC
(Unlimited Release)